1-1-2009

Thermo-solutal convection with Soret effect

Md. Abdur Rahman
Ryerson University

THERMO-SOLUTAL CONVECTION WITH SORET EFFECT

by

Md. Abdur Rahman

B.Sc. in Mechanical Engineering, KUET, Bangladesh, 2007

A thesis

presented to Ryerson University

in partial fulfillment of the

requirement for the degree of

Master of Applied Science

in the Program of

Mechanical Engineering

Toronto, Ontario, Canada, 2008

Author Declaration

I hereby declare that I am the sole author of this thesis or dissertation.

I authorize Ryerson University to lend this thesis or dissertation to other institutions or individual for the purpose of scholarly research.

I further authorize Ryerson University to reproduce this thesis or dissertation by photocopying or by other means, in total or in part, at the request of other institutions or individuals for the purpose of scholarly research.

ABSTRACT

THERMO-SOLUTAL CONVECTION WITH SORET EFFECT

Md. Abdur Rahman

Master of Applied Science

Mechanical and Industrial Engineering, 2008

School of Graduate Studies

Ryerson University, Toronto, On, M5B 2K3, Canada

In the present study, the onset of thermal convection in a liquid layer overlying a porous layer where the whole system is being laterally heated is investigated. The non-linear two-dimensional Navier Stokes equations, the energy equation, the mass balance equation and the continuity equation are solved for the liquid layer. Instead of the Navier Stokes equations, the Brinkman model is used for the porous layer. The partial differential equations are solved numerically using the finite element technique. A two-dimensional geometrical model with lateral heating is considered. Two different cases are analyzed in this thesis. In the first case, the gravity driven buoyancy convection and the Marangoni convection are studied. For the Marangoni convection, the microgravity condition is considered and the surface tension is assumed to vary linearly with temperature. Different aspect ratios, as well as thickness ratios, are studied in detail for both the buoyancy and the Marangoni convection. Results revealed that for both the buoyancy and the Marangoni cases, flow penetrates into the porous layer, only when the thickness ratio is more than 0.90. In the case of thermo-solutal convection in the presence of Soret effect, it has been found that the isopropanol component goes either towards the hot or the cold walls depending on the fluid mixtures which has been used in the system.

Borrower

Ryerson University requires the signatures of all persons using or photocopying this thesis. Please sign below, and give address and date.

ACKNOLEDGEMENTS

The author would like to sincerely thank Prof. Dr. Ziad Saghir of Ryerson University for his helpful assistance, guidance and encouragement throughout the completion of this thesis. Without his help, it was quite impossible for the author to complete this thesis. The author would also like to express his appreciation to both of his parents Md. Abu Bakar Sheikh and Sarifunnesa Begum for their support. The author also acknowledges the support and useful suggestions of his colleagues T. Jaber and M. M. Shemirani, PhD students of Ryerson University.

TABLE OF CONTENTS

LIST OF TABLES

LIST OF FIGURES

NOMENCLATURE

AR	Aspect ratio = $\frac{H}{L}$
Bi	Biot number
c	Concentration of the fluid
C	Non-dimensional concentration of the fluid
$(C_p)_f$	Specific heat of liquid at constant pressure
d	Thickness ratio = $\frac{d_2}{L}$
d_1	Liquid Layer thickness
d_2	Porous layer thickness
D_M	Solutal diffusion coefficient
D_T	Thermal diffusion coefficient
g	Gravitational acceleration
G	Non-dimensional overall thermal conductivity
H	Length of cavity in horizontal X-direction
k_f	Conductivity of the fluid
k_s	Conductivity of the solid glass beads
k_e	Effective thermal conductivity
L	Characteristic length of the cavity in Y-direction=d_1+d_2
p	pressure
P	Non-dimensional pressure = $\frac{p.L}{\mu.u_o}$
q	Separation ratio = $\frac{(c/(1-c))_{Max}}{(c/(1-c))_{Min}}$

Q Heat flux

S_T Soret coefficient $= \frac{D_T}{D_M}$

t time

T Temperature

Δc Initial concentration difference

ΔT Temperature difference between lateral walls = T_H - T_C

u Velocity component in the x direction

U Non-dimensional velocity component in the X direction = $\frac{u}{u_o}$

u_o Characteristic velocity = $\sqrt{g.\beta_T.\Delta T.L}$

v Velocity component in the y direction

V Non-dimensional velocity component in the Y direction = $\frac{v}{u_o}$

V_t Total volume

V_f Volume occupied by the fluid

V_s Volume occupied by the solid

Non-dimensional numbers

Da Darcy number = $\frac{\kappa}{L^2}$

Ma Marangoni number = $\frac{|\gamma|.(\Delta T).L}{\alpha.\mu}$

Pr Prandtl number = $\frac{\nu}{\alpha}$

Ra_{LC} Solutal Rayleigh number for liquid layer= $\frac{g.\beta_C.\Delta C.d_1^3}{\nu.\alpha}$

Ra_{LL} Thermal Rayleigh number for liquid layer = $\frac{g.\beta_T.\Delta T.d_1^3}{\nu.\alpha}$

Ra_{PC} Solutal Rayleigh number for porous layer= $\frac{g.\beta_C.\Delta C.d_2.\kappa}{\nu.\alpha}$

Ra_{PL} Thermal Rayleigh number for porous layer= $\frac{g.\beta_T.\Delta T.d_2.\kappa}{\nu.\alpha}$

Re Reynolds number = $\frac{\rho_O.u_o.L}{\mu}$

Sc Schmidt number = $\frac{\nu}{D_M}$

Greek Symbols

α Thermal diffusivity = $\frac{k_f}{\rho_O.(C_p)_f}$

α_T Soret effect= $T.S_T$

β_C Solutal expansion

β_T Thermal volume expansion

γ Surface tension gradient

θ Non-dimensional temperature = $\frac{T-T_C}{\Delta T}$

κ Permeability

τ Non-dimensional time

τ_D Diffusive characteristic time

τ_{th} Thermal characteristic time

τ_D Diffusive characteristic time

μ Dynamic viscosity

ν Kinematic viscosity

ρ_O Density of the fluid at reference temperature T_O

σ Stress

σ_m Non-dimensional surface tension

ϕ Porosity

Ψ Stream function

$\Delta\Psi$ Streamline difference between two plot contours

Subscripts

C Cold

e Effective

f Fluid

H Hot

L Liquid

O Reference

P Porous

CHAPTER 1

Introduction and Literature Review

1.1 Introduction

A vertically stacked system of porous and fluid layers, with heat and mass transfer taking place through the interface, is related to many natural phenomena and various industrial applications. The related problem of a liquid layer overlying a porous layer is also found in many environmental and engineering applications as well. The water layer of a pond or a lake with a muddy bottom layer, transport phenomena that occurs from soil to water and vice versa, the geothermal system are some of the examples of environmental applications. The thermodiffusion effect or the Soret effect is the mass flux in a mixture due to a temperature gradient. This effect is very weak but can be important in the analysis of compositional variation in hydrocarbon reservoirs.

1.2 Literature Review

1.2.1 Onset of gravity driven and Marangoni convection

Saghir *et al.* [1] studied Marangoni and gravity driven convection in a liquid layer overlying a porous layer. They analyzed the onset of thermal convection for both the bottom and lateral heating conditions. For the bottom heating case, they found that when natural convection was in the liquid layer, the aspect ratio changed the flow configuration. However, when the natural convection was in the porous layer, the aspect ratio had no effect on the flow pattern. They also found that large convective motion was present for a low thickness ratio and weakens as the

thickness ratio increased further. For both bottom and lateral heating cases, they found that the liquid layer thickness determines whether the flow is dominant in the liquid layer or in the porous layer and in some cases multi-cell formation occurs due to changing of the aspect ratio.

Nield and Bejan [2] devoted a collection of their works in the area of convection in porous media in their book. They defined a porous medium as a material consisting of a solid matrix with an interconnected void. The solid matrix is either rigid or undergoes small deformations. The interconnectedness of the void (the pores) allows the flow of one or more fluids through the material. They defined the porosity ϕ, as the fraction of total volume of the medium that is occupied by void space, or the liquid in this present case. So 1- ϕ is the fraction occupied by the solid beads. Within V_t, let V_f represent the volume occupied by the fluid and V_s represent the volume occupied by the solid, where $V_t = V_f + V_s$. Then the porosity of the porous medium can be defined as $\phi = \frac{V_f}{V_t}$.

Nield [3] first formulated the onset of convection in a fluid layer overlying a porous layer. He proposed an analytic solution including the Marangoni effect at a deformable upper surface. He found that the Marangoni and gravity effects are additive for the onset of convection in a fluid layer overlying a porous medium.

Birikh [4] studied the effect of thermo capillary on convection in a horizontal liquid layer. He calculated the critical characteristic thickness for some liquids. He found that the convection was purely thermal when the thickness of the liquid layer was greater than the critical value and largely capillary when the thickness of the liquid layer was less than the critical value.

Villers and Platten [5] analyzed the convection in acetone due to the coupled buoyancy and Marangoni case. From their numerical simulations, they found that, with fluids of Prandtl

number much greater than one, temperature fluctuations constitute dangerous sources of instability.

Pearson [6] investigated the convection cells which were induced by surface tension. He found that two factors tending to instability would be relevant. The first one is due to temperature variations and the second is due to relative concentration variations. He also found that surface tension forces are responsible for cellular motion in many cases where the criteria given in terms of buoyancy forces would not allow for instability.

Kozak *et al.* [7] studied Marangoni convection in a liquid layer overlying a porous layer taking into consideration evaporation at the free surface. They studied different aspect ratios, thickness ratios and temperatures for the pure thermocapillary case. For lateral heating case, they found that switching of the flow from the liquid layer into the porous layer is due to the ratio of liquid thickness to the porous thickness. Also, they found that, for thermocapillary flow without evaporation, multi cell formation occurs by changing the aspect ratio. Their analysis showed that evaporation has a strong effect on the convection cell pattern in both liquid and porous dominant flow. They also verified that the two-dimensional flow model is a good representation of the three-dimensional situation.

Hadid and Roux [8] analyzed thermocapillary convection of low Prandtl number liquids subjected to a horizontal temperature gradient in a lateral heating cavity. They observed that, for the case with low-Prandtl number fluids ($Pr = 0.015$), the flow field is almost independent of the temperature field. For an aspect ratio $A = 4$, they found that the flow field and the surface velocity were the same for both insulating and conducting horizontal walls. Also, they found that, for a small Reynolds number the flow reached the fully developed Poiseuille-Couette flow

solution in the central region of the cavity. But, for high Reynolds number, the length of the region of fully developed Poiseuille-Couette flow was reduced and even disappeared.

Schwabe *et al.* [9] observed the multi-roll-structure of thermocapillary flow for a thin liquid layer. They studied a microgravity experiment for thermocapillary flow structures without coupling to buoyancy in a 20.0 mm wide annular layer with a free surface of variable depth heated by the outer wall and cooled at the inside. They found that the multi-roll was dominated by thermocapillarity for the layers with thickness up to 5 mm. Also, a variety of flow structures were found for the thin fluid layers with a free flat surface and a temperature gradient parallel to it.

Schwabe [10] studied the Marangoni convection instability in small circular containers under the microgravity condition. He observed the instability during the 12 minute microgravity-phase of a 3.0 mm thick layer of silicone oil heated from below. He showed some pictures of the flow structures of the instabilities. He found that the flow structure at t = 334.5 seconds after launch, convection developed in all containers but rather structureless compared to later times.

Mokhtar *et al.* [11] analyzed the Marangoni convection in a fluid saturated porous layer heated from below. They obtained the closest form of an analytical solution for the onset of steady Marangoni convection in a fluid saturated porous layer. They found that the Marangoni numbers depend on the Darcy number and the Biot number. They also found that the critical Marangoni number increases as the Darcy number increases.

Bahloul *et al.* [12] studied surface tension effect on convection in a binary fluid layer under a zero gravity environment. They found that the different flow regimes depend on the thermal and solutal Marangoni numbers. Also, they found that the parallel flow approximation is in good

agreement with the numerical results, independently of the strength of the convective motion, in the range of the parameters considered in their study.

Delache and Ouarzazi [13] observed mixed convection patterns in a bottom heated porous media. In the case of convective instability, they obtained an analytical criterion which specifies the conditions about the observability of their *T* modes (moving three dimensional modes) or *L* rolls (stationary longitudinal rolls) at the onset of convection. They also examined how their predictions are modified in the presence of some permanent disturbances located at the entrance cross section of the channel. Their numerical solutions showed that the mixed mode is composed with the two types of pattern at the same spatial location.

Kandaswamy and Eswaramurthi [14] studied numerically the buoyancy-driven convection of water in a porous cavity with variable side wall temperatures. They found that the strength of convection and the heat transfer rate become weak due to more flow restriction in the porous medium for small porosity. They found that, when the Darcy number is small, the heat transfer takes place by the mode of conduction. The convective heat transfer rate goes down as the Darcy number decreases. They also observed that the Darcy number, which depends on the permeability of the porous medium, has strong effects on convection in the porous-filled cavity. The motion of the fluid particle is higher for higher values of the Darcy number and the flow is restricted largely in the case of very low values of Darcy number.

Kim and Choi [15] investigated the effects of the Rayleigh number, aspect ratio and thickness ratio on convection in the composite layer of a bottom heated porous layer and an overlying fluid layer. They found that, at the supercritical Rayleigh number regime (when the depth ratio, $d >$ 0.12), the number of recirculating cells increase continuously as the Rayleigh number increases, which in turn increases the Nusselt number. For that depth ratio range, convection was limited to

the fluid layer, while conduction was the dominating heat transfer mode in the porous layer. For $d = 0.10$, the recirculating cells were continuously readjusting their positions and sizes in the composite layer as the Rayleigh number increases.

Chen & Chen [16] studied convective stability in bottom heated superposed fluid and porous layers. The depth ratio d, which is the ratio of the thickness of the fluid layer to that of the porous layer, was varied from 0 to 1.0. They detected the onset of convection by changing the slope in the heat flux curve. Their results showed a decrease in the critical Rayleigh number as the depth of the fluid layer is increased from zero. They confirmed the sudden decrease in the critical wavelength between $d = 0.10$ and 0.20 (as predicted by the linear theory) by temperature measurements and by the pattern exhibited in the liquid crystal film. They also found that the convection cells were generally three dimensional.

Desaive *et al.* [17] analyzed instability of a coupled capillary and gravity driven liquid film overlying a porous layer. Their aims were to develop the linear stability analysis of a porous-liquid bilayer system. Instead of Darcy's law, they used the Brinkman model for their analysis. They assumed that the upper fluid boundary was either rigid or free and would include a Marangoni effect. For the short wave mode, they found that convection takes place only in the fluid region. They also found that Brinkman's model gives qualitatively the same results as Darcy's law. Indeed, the effective viscosity introduced in Brinkman's approach didn't significantly affect the critical stability conditions. The critical depth ratio disappeared at very large and at very small Darcy numbers. In the pure thermocapillary case, they found that convection was confined to the fluid layer except for the very small fluid depth.

Shivakumara *et al.* [18] studied surface-tension-driven convection in a two-layer system comprising an incompressible fluid-saturated porous layer over which laid a layer of the same

fluid. They investigated the effect of variation of different physical parameters on the onset of Marangoni convection. They found that the ratio of the thickness of the fluid layer to that of the porous layer have a profound effect on the stability of the system. They also found that the decrease in *Da* (Darcy number) increases the critical Marangoni numbers, thus making the system more stable.

Smith and Davis [19] analyzed convective instabilities of a dynamic thermocapillary liquid layer. They found that an increase in Biot number (B) always results in an increase of the Marangoni number (Ma) in the system. When $B = 0$, the minimum Marangoni number over the neutral surface is a function of Pr only. They also found that as the Prandtl number of the fluid decreases, the critical Marangoni number and the critical wave number of the instability increase. The results of their analysis showed that the increasing behavior of Ma_C with decreasing Pr is due to the stabilizing effect of heat convection by horizontal velocity perturbations. But when Ma is fixed, an increase in Pr would cause an increase in vertical convection and the layer becomes unstable. As a result, Ma_C decreases as Pr increases.

Hooman and Gurgenci [20] studied the Benard convection in a porous medium using a non-Darcy model. They studied the effects of fluid viscosity variation on isotherms, streamlines, and the Nusselt number. They examined the application of the effective and average Rayleigh number. With a fixed value of *Da* (Darcy number), they found that an increase in either Ra (Raleigh-Darcy number, $Ra = Da.Ra_f$) or Ra_f (fluid Raleigh number) leads to stronger convective flows. They found that the reference temperature at which the fluid properties should be evaluated is a decreasing function of the Darcy number and is approximately independent of the other parameters. They recommended that, by applying this reference temperature, anyone can reduce the computational time and expense required for solving a variable property problem.

Silberstein *et al.* [21] examined the onset criteria of natural convection in fibrous insulating materials with permeable interfaces. They studied two configurations of practical interest for the building industry either with or without an impermeable fluid-porous interface: a vertical porous layer placed in between two fluid cavities and a horizontal fluid-porous layer system representative of an insulated attic in the winter time. In the horizontal bi-layer configuration (with ascendant heat flow), they found that convection sets in the porous insulant. They also found that the thermal consequences of the early fluid motion are directly connected to the flow dynamics of the fluid layer above the insulant. But a serious degradation of the thermal properties of the insulation seems to occur only for highly permeable products such as loose-fills placed under very severe climatic conditions. For the evolution of the global heat flow through the system with the temperature gradient, the behavior of the three-layer system depends strongly on the permeability of the fluid-porous interface. Their experimental and numerical data showed that the sensibility of porous materials to convection depends strongly on the boundary conditions (isothermocity, permeability etc.) of the fluid-porous interface.

1.2.2 Onset of Thermo-solutal Convection with Soret Effect

Saghir *et al.* [22] investigated double diffusive and Marangoni convection in a multi-cavity system. They numerically investigated the interaction between the Marangoni convection and the double diffusive convection. They solved the problem for two different cases. In the first case, they assumed that the upper horizontal surface was a fixed wall, and in the second case, the upper horizontal wall was a free surface in order to study the thermal and solutal interface tension gradient effect at the free surface. From their analysis, they found that the double diffusive convection plays a major role in the intrusion of the salted water into fresh water. They

also found that the temperature and salinity induce a strong convection. In addition, they found that, when a free surface exists in the system, other surface forces namely the thermal and solutal Marangoni convection enhances convection.

Tanny and Yakubov [23] investigated the mixing process of a double-diffusive two-layer system in a laterally heated enclosure. They found that for the lateral heating enclosure, a circulating flow was induced in each layer such that the interface separating the layers was simultaneously exposed to destabilizing the shear and double diffusive convection. Their results showed that when the flow adjacent to the interface was unstable, the mixing time was relatively short. On the other hand, when the interfacial flow was stable, no vortices existed at the interface and the mixing time was much longer. They also found that the appearance of vortices at the interface separating the layers is an instability phenomenon. The critical Rayleigh number for the onset of interfacial instabilities increases with the buoyancy ratio (solutal Rayleigh number) of the system. And for given buoyancy ratio, the non-dimensional mixing time for stable experiments is larger than for unstable experiments. Also, they found that, for both stable and unstable conditions, the non-dimensional mixing time increases with the buoyancy ratio of the system.

Jiang *et al.* [24] studied thermo-gravitational convection for a binary mixture of methane and n-butane in a vertical porous column. Their numerical results revealed that the lighter fluid component migrated to the hot side of the cavity. Also, they found that, as the permeability increases, the component separation in the thermal diffusion or Soret effect process increases, reaches its peak and then decreases. They explained the convection effect on the thermal diffusion in a hydrocarbon binary system in terms of the characteristic times. When the characteristic time of the convective flow is larger than the characteristic time of the thermal diffusion, then the Soret effect is the dominant force for the composition separation in the cavity

and maximum separation is reached when the characteristic time is equal to the time of thermal diffusion. And when the characteristic time is less than the time of thermal diffusion, the buoyancy convection becomes dominant and that corresponds to permeability greater than 10 md.

Bergeon *et al.* [25] investigated numerically the Marangoni convection with Soret effect in a binary mixture. They found that, for the large Soret coefficient, convection is initiated by solutal effects and leads to a single large roll. They found that, as the Marangoni number increases, the one-roll states are succeeded by two-roll states with up flow in the centre of the cell. They also found that for *Ma* (Marangoni number) between the thermal-solutal and thermal thresholds, a weak convective flow (the Soret regime) exists. For *Ma* higher than the pure thermal threshold, a much stronger flow resembles convection in a pure fluid and the concentration field was mixed (the Marangoni regime). They found that, for larger S_M (Marangoni Soret parameter), the branches which are the first to bifurcate may terminate while still in the Soret regime. However, they found that, for negative S_M, the distinction was more complicated than for positive S_M: the Soret branches were unstable and co-exist with stable Marangoni branches.

Mansour *et al.* [26] studied the thermosolutal convection developed in a horizontal shallow porous layer salted from below and subject to a cross flux of heat. They studied the combined effect of thermodiffusion and lateral heating on double diffusive natural convection in a horizontal porous layer, filled with a binary fluid and subjected to uniform fluxes of heat and mass on its long sides. Their obtained results showed that the φ-N (where φ is separation ratio and N is the buoyancy ratio) plane can be divided into four regions with different characteristics in terms of multiplicity of solutions. They also found that the increase of Soret parameter (φ)

above some threshold leads to the disappearance of the multiplicity of solutions. Finally, they recommended that the Soret effect may modify considerably the heat transfer.

Jiang *et al.* [27] simulated the Ludwig-Soret effect of a water-ethanol mixture in a cavity filled with aluminum oxide powder under high pressure. They analyzed the thermal diffusion or Soret effect, globally with a separation ratio and locally with the distributions of ethanol mole fraction, on the horizontal and vertical lines in the center of the porous cavity. They found that, when the value of permeability was less than 10^4 md, the composition separation in the cavity was evident, and when the value of permeability was larger than10^4 md, the thermosolutal convection created a mixing of the substances and the separation is diminished. From their investigation, they found that the thermal conductivity of aluminum oxide has no significant effect on the compositional separation at the steady state of the thermosolutal convection.

Benano-Melly *et al.* [28] modeled a thermogravitational experiment in a laterally heated porous medium. They showed that, when solutal and thermal buoyancy forces oppose each other, multiple convection-roll flow patterns develop. They investigated the solutal buoyancy force, combined solutal and thermal buoyancy forces, and counteracting solutal and thermal buoyancy forces for both the positive and the negative Soret numbers. They showed that the separation ratio increases with increasing Lewis number and Soret number. They also showed that the separation ratio increases with increasing aspect ratio. However the separation ratio increases with increasing thermal Rayleigh number, reaches its peak and then decreases.

Platten [29] studied the Soret effect of an elementary Soret cell. His results were provided for several systems, with both negative and positive Soret coefficients, and comparison between several laboratories was made for the same systems. In earth conditions, five European labs decided to investigate independently the same systems, i.e., same chemical compounds from the

same batch with the same purity, same composition, and same temperature. After two years of individual work, the comparison of results produced by different labs showed that the benchmark campaign was a success. The highest difference from the mean was only 7% for one particular system. Therefore, they (the five European labs) were able to propose benchmark values, and they deny the need sometimes expressed to go to microgravity for measuring Soret coefficients, at least for usual organic mixtures near room temperature.

Alexandrov and Aseev [30] analyzed the thermodiffusion and temperature-dependent diffusivity of a binary melt. They found that the concentration and temperature fields in the liquid, solid and mixed state phases are functions of all thermophysical parameters. They determined the rate of solidification and two-phase zone thickness. Their theory demonstrated that the mushy zone could be treated as a self-similar object. From their study, they found that the thermodiffusion and temperature dependent diffusivity modifying the heat and mass transfer are essential. They also found that the influence of the Soret effect on the crystallization process was characterized by the sign of the thermodiffusion coefficient.

Er-Raki *et al.* [31] studied thermosolutal convection induced in a vertical porous medium. They studied analytically and numerically the thermosolutal natural convection induced in a vertical porous layer heated and salted with uniform fluxes. They found that for a particular situation, where the external mass flux is compensated by the Soret effect, the boundary layer regime remains absent in the case of concentration independently of the governing parameters.

Ming-chun *et al.* [32] investigated Soret (mass transfer caused by the temperature gradient) and Dufour (heat transfer caused by the concentration gradient) effects in a strongly endothermic chemical reaction system of porous media. They discussed the influence of the Soret and Dufour effects on the heat transfer, mass transfer and the chemical reaction in the porous medium. They

Chapter 2

Mathematical Formulation and Numerical Approach

2.1 Model Description

The schematic diagram for this study is illustrated in Figure 2.1. It represents a two-dimensional rectangular cavity split into a liquid layer and a porous layer. The incompressible liquid layer, whose solutal expansion is β_C and thermal expansion coefficient is β_T, has a height of d_1 and a width of H. The physical properties of the liquid are assumed constant. The top wall of the liquid layer is a non-deformable free surface. The liquid layer overlays a homogeneous and rectangular porous layer that is saturated with the liquid. It is assumed that the liquid and the porous layer are in thermal equilibrium. The porous matrix has a porosity = 0.39, which corresponds to glass bead of 3.25 mm diameter. The Darcy number is set to a constant of Da = 1.0E-05 for the entire analysis. The porous layer has the same width of H and a height of d_2. The total thickness is defined by $L = d_1+d_2$.

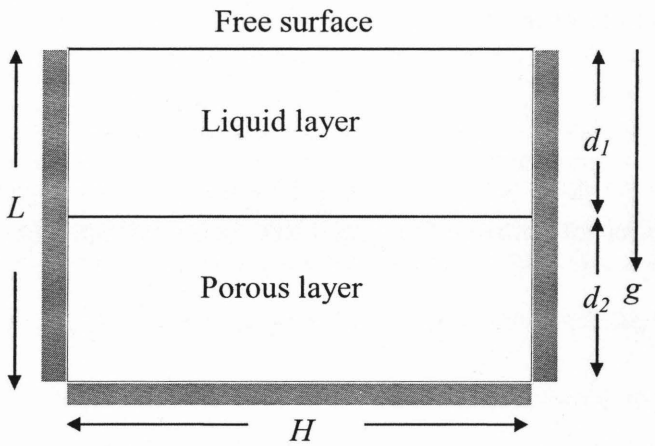

Figure 2.1 Geometrical model of the two-dimensional cavity

analyzed the reaction features of packed bed of pellets under different conditions by varying the key parameters. Their calculated results showed that, when the convectional velocity is lower or when the initial temperature of the feeding gas is higher, the Soret and Dufour effects can't be ignored. They found that both the temperature field of the bulk flow and the solid fractional conversion increases with an increase in the convection velocity or in the initial temperature of the feeding gas. The concentration distribution of the product gas decreases with an increase in the convection velocity and increases with the initial temperature of the feeding gas.

1.3 Research objective

The objective of this research is to investigate the onset of thermal convection in a liquid layer overlying a porous layer, where the whole system is laterally heated. Several cases are considered for this research. First, pure buoyancy and Marangoni convection are analyzed for different thickness ratios, aspect ratios, Rayleigh numbers, Marangoni numbers and Prandtl numbers. Then, thermo-solutal convection with transient condition is studied by taking into consideration the molecular diffusion effect. Finally, thermo-solutal convection with thermodiffusion or Soret effect in reduced gravity condition is studied.

For the entire analysis, the height of the cavity, L = 0.01m. The aspect ratio is the ratio of width of the cavity to its thickness, $AR = H/L$ and will be studied throughout the thesis. The gravitational acceleration term is set to act in the negative Y-direction.

2.2 Liquid Layer Governing Equations

The flow under consideration is assumed laminar and incompressible. The model is presented in Cartesian coordinates. The complete continuity, momentum balance, energy balance and mass balance equations are solved simultaneously in order to study the convection patterns. Using the finite element technique, the equations are solved numerically for both the liquid layer and the porous layer of the cavity. Following are the governing equations, boundary conditions and numerical procedure used for the various cases in this study. The equations are presented for the two-dimensional transient model, but similar equations without the t (time) term are used for the steady state model. The dimensional and non-dimensional equations are explained in detail in Appendix A.

2.2.1 Continuity Equation

The equation of continuity is a partial differential equation which represents the conservation of mass for an infinitesimal control volume. The continuity equation for an incompressible fluid is given by:

$$\left[\frac{\partial u}{\partial x}+\frac{\partial v}{\partial y}\right]=0 \tag{2.1}$$

2.2.2 Momentum Balance Equation

For the liquid layer, the momentum balance equation is represented by the Navier-Stokes equations. The flow model is Newtonian, incompressible and steady or transient. In the x direction, the principle of conservation of linear momentum dictates that:

$$\rho_O\left[\frac{\partial u}{\partial t}+u\frac{\partial u}{\partial x}+v\frac{\partial u}{\partial y}\right]=-\frac{\partial p}{\partial x}+\mu\left[\frac{\partial^2 u}{\partial x^2}+\frac{\partial^2 u}{\partial y^2}\right] \tag{2.2}$$

In the y direction, the momentum equation is written as follow:

$$\rho_O\left[\frac{\partial v}{\partial t}+u\frac{\partial v}{\partial x}+v\frac{\partial v}{\partial y}\right]=-\frac{\partial p}{\partial y}+\mu\left[\frac{\partial^2 v}{\partial x^2}+\frac{\partial^2 v}{\partial y^2}\right]-\rho_O.g.[\beta_T(T-T_O)-\beta_C(c-c_O)] \tag{2.3}$$

The Boussinesq approximation in the momentum equation in the y-direction allows for modeling of buoyancy effects for an incompressible fluid. The Boussinesq approximation has the following two assumptions: the variations in fluid density affect only the buoyancy term; the fluid density is a function of temperature and species concentration only [33].

2.2.3 Energy balance Equation

The thermal energy conservation equation assuming Φ = 0, for an incompressible fluid is expressed as:

$$\rho_O.(C_p)_f.\left[\frac{\partial T}{\partial t}+u.\frac{\partial T}{\partial x}+v.\frac{\partial T}{\partial y}\right]=k_f\left[\frac{\partial^2 T}{\partial x^2}+\frac{\partial^2 T}{\partial y^2}\right] \tag{2.4}$$

2.2.4 Mass Balance Equation

The mass balance equation for the species can be expressed as:

$$\rho_O \cdot \left[\frac{\partial c}{\partial t} + u \frac{\partial c}{\partial x} + v \frac{\partial c}{\partial y} \right] = \rho_O . D_M \cdot \left[\frac{\partial^2 c}{\partial x^2} + \frac{\partial^2 c}{\partial y^2} \right] + \rho_O . D_T \cdot \left[\frac{\partial^2 T}{\partial x^2} + \frac{\partial^2 T}{\partial y^2} \right] \tag{2.5}$$

In the above equations, u and v represent the velocities in the x and y directions in a Cartesian coordinate system. The p, ρ_O, μ, β_T, β_C, T, and g are the pressure, density of the fluid at reference temperature T_O, dynamic viscosity, coefficient of thermal expansion associated with temperature variations, coefficient of solutal expansion associated with concentration variations, temperature and gravitational acceleration, respectively. Also $(C_P)_f$, k_f, D_M and D_T denote the specific heat at constant pressure, the conductivity of the fluid, the molecular diffusivity and the thermal diffusion coefficient of the fluid, respectively.

2.3 Porous Layer Governing Equations

For the saturated porous matrix, the Brinkman model is used. Following are the continuity, momentum balance, energy balance and mass balance equations for the porous medium.

2.3.1 Continuity Equation

As the fluid is incompressible, the continuity equation for the porous layer is also given by:

$$\left[\frac{\partial u}{\partial x} + \frac{\partial v}{\partial y} \right] = 0 \tag{2.6}$$

2.3.2 Momentum Balance Equation

Darcy was the first to formulate the basic equation of flow in porous media based on the proportionality between the flow rate and the applied pressure difference that was revealed from experiment. Conventionally, Darcy's law was used as the momentum balance equation in a

porous medium. However, as noted by Deasive *et al.* (2001), it suffers from mathematical inaccuracy due to the inability to impose a no-slip boundary condition. Consequently, in this study, the Brinkman equation is used to represent the momentum equation. In the x direction, the momentum equation is written as follows:

$$\frac{\rho_O}{\phi}.\left[\frac{\partial u}{\partial t}\right]+\frac{\mu}{\kappa}.u=-\frac{\partial p}{\partial x}+\mu.\left[\frac{\partial^2 u}{\partial x^2}+\frac{\partial^2 u}{\partial y^2}\right] \tag{2.7}$$

In the y direction, the momentum equation is represented by:

$$\frac{\rho_O}{\phi}.\left[\frac{\partial v}{\partial t}\right]+\frac{\mu}{\kappa}.v=-\frac{\partial p}{\partial y}+\mu.\left[\frac{\partial^2 v}{\partial x^2}+\frac{\partial^2 v}{\partial y^2}\right]-\rho_O.g.[\beta_T(T-T_O)-\beta_C(c-c_O)] \tag{2.8}$$

Here, the permeability is denoted by κ in the Darcy term on the left hand side of the above equations (2.7)-(2.8). The Brinkman form of the momentum equation is suitable when one wants to match a solution in a porous medium and in an adjacent viscous fluid. The Brinkman extension is added as the second term on the right hand side of the above equations.

2.3.3 Energy Balance Equations

The energy balance equation for the porous layer is given by:

$$\rho_O.(C_p)_f.\left[u.\frac{\partial T}{\partial x}+v.\frac{\partial T}{\partial y}\right]=k_e\left[\frac{\partial^2 T}{\partial x^2}+\frac{\partial^2 T}{\partial y^2}\right] \tag{2.9}$$

In addition to the governing equation, the following constitutive thermal relationship is used for the overall thermal conductivity:

$$k_e=\phi.k_f+(1-\phi).k_s \tag{2.10}$$

Where, k_e is the effective thermal conductivity, k_f is the conductivity of the fluid and k_s is the conductivity of the solid. The effective thermal property is related to the fluid and solid matrix properties by the relation in equation (2.10). The porosity is denoted by ϕ. In general, the dynamic viscosity μ and the effective dynamic viscosity μ_e are only approximately equal to each other. However, the Brinkman approximation sets the viscosity and the effective viscosity equal to each other.

2.3.4 Mass Balance Equation

The mass balance equation for the species can be expressed as:

$$\rho_O \cdot \left[\frac{\partial c}{\partial t} + u.\frac{\partial c}{\partial x} + v.\frac{\partial c}{\partial y}\right] = \rho_O . D_M \cdot \left[\frac{\partial^2 c}{\partial x^2} + \frac{\partial^2 c}{\partial y^2}\right] + \rho_O . D_T \cdot \left[\frac{\partial^2 T}{\partial x^2} + \frac{\partial^2 T}{\partial y^2}\right] \tag{2.11}$$

2.4 Non-Dimensional Analysis

Non-dimensional formulation of the governing equations has many advantages. Scaling variables and assembling the non-dimensional parameters provides a measure of the importance of the various terms in the equations and identifies the dominant physical phenomena [34]. Equations (2.1) – (2.11) were rendered dimensionless by using the following non-dimensional groups:

$$U = \frac{u,}{u_O}, V = \frac{v}{u_O}, X = \frac{x}{L}, Y = \frac{y}{L}, P = \frac{pL}{\mu u_O}, u_O = \sqrt{g\beta_T \Delta T L}, \tau = \frac{tu_O}{L}, \theta = \frac{T - T_O}{L},$$

$$C = \frac{c - c_O}{\Delta c}, L = d_1 + d_2, \mathrm{Re} = \frac{\rho_O u_O L}{\mu}, \mathrm{Pr} = \frac{\nu}{\alpha}, Da = \frac{\kappa}{L^2}, Ra_{LL} = \frac{g\beta_T \Delta T d_1^3}{\nu\alpha},$$

$$Ra_{LC} = \frac{g\beta_C \Delta C d_1^3}{\nu\alpha}, Ra_{PL} = \frac{g\beta_T \Delta T d_2 \kappa}{\nu\alpha}, Ra_{PC} = \frac{g\beta_C \Delta C d_2 \kappa}{\nu\alpha}, Sc = \frac{\nu}{D_M} \tag{2.12}$$

Where U, V, X and Y are the non-dimensional x and y component of velocity, and non dimensional x and y coordinates, respectively. P is the non-dimensional pressure term and θ is

the non-dimensional temperature term. The characteristic length, temperature and velocity are denoted by L, T, and u_O. In the non-dimensional analysis, several other parameters appear, such as the Reynolds number Re, the Prandtl number Pr, the Darcy number Da, thermal Raleigh number for the liquid layer Ra_{LL}, solutal Raleigh number for the liquid layer Ra_{LC}, thermal Raleigh number for the porous layer Ra_{PL}, solutal Raleigh number for the porous layer Ra_{PC}, Schmidt number Sc. The parameters in equation (2.12) are used in the analysis, which are fully outlined in Appendix A. The governing equations in the dimensionless form are described in the sections below.

2.5 Non-Dimensional Liquid Layer Governing Equations

2.5.1 Continuity Equation

$$\left[\frac{\partial U}{\partial X}+\frac{\partial V}{\partial Y}\right]=0 \tag{2.13}$$

2.5.2 Momentum Balance Equation

The Navier-Stokes Equations for the X and Y directions are given as follows:

***X* direction:**

$$\mathrm{Re}.\left[\frac{\partial U}{\partial \tau}+U.\frac{\partial U}{\partial X}+V.\frac{\partial U}{\partial Y}\right]=-\frac{\partial P}{\partial X}+\left[\frac{\partial^2 U}{\partial X^2}+\frac{\partial^2 U}{\partial Y^2}\right] \tag{2.14}$$

***Y* direction:**

Without thermodiffusion

$$\mathrm{Re}.\left[U.\frac{\partial V}{\partial X}+V.\frac{\partial V}{\partial Y}\right]=-\frac{\partial P}{\partial Y}+\left[\frac{\partial^2 V}{\partial X^2}+\frac{\partial^2 V}{\partial Y^2}\right]-\mathrm{Re}.\theta \tag{2.15}$$

Including thermodiffusion

$$\mathrm{Re}.\left[\frac{\partial V}{\partial \tau}\right]+\frac{1}{Da}[V]=-\frac{\partial P}{\partial Y}+\left[\frac{\partial^2 V}{\partial X^2}+\frac{\partial^2 V}{\partial Y^2}\right]-\left[\frac{1}{\mathrm{Pr}.\mathrm{Re}.Da}\right].(1+\frac{d_2}{d_1})^3.[Ra_{PL}.\theta-Ra_{PC}.C] \tag{2.16}$$

2.5.3 Energy Balance equation

$$\mathrm{Re}.\mathrm{Pr}.\left[\frac{\partial \theta}{\partial \tau}+U.\frac{\partial \theta}{\partial X}+V.\frac{\partial \theta}{\partial Y}\right]=\left[\frac{\partial^2 \theta}{\partial X^2}+\frac{\partial^2 \theta}{\partial Y^2}\right] \tag{2.17}$$

2.5.4 Mass Balance Equation

Mass balance Equation for the species without thermodiffusion is:

$$\left[\frac{\partial C}{\partial \tau}+U.\frac{\partial C}{\partial X}+V.\frac{\partial C}{\partial Y}\right]=\frac{1}{\mathrm{Re}.Sc}.\left[\frac{\partial^2 C}{\partial X^2}+\frac{\partial^2 C}{\partial Y^2}\right] \tag{2.18}$$

With thermodiffusion is:

$$\left[\frac{\partial C}{\partial \tau}+U.\frac{\partial C}{\partial X}+V.\frac{\partial C}{\partial Y}\right]=\frac{1}{Sc}.\sqrt{\frac{\mathrm{Pr}}{Ra_{LL}}}.\left[1+\frac{d_2}{d_1}\right]^{-\frac{3}{2}}\left\{\left[\frac{\partial^2 C}{\partial X^2}+\frac{\partial^2 C}{\partial Y^2}\right]+\alpha_T.\left[\frac{\partial^2 \theta}{\partial X^2}+\frac{\partial^2 \theta}{\partial Y^2}\right]\right\} \tag{2.19}$$

2.6 Non Dimensional Porous Layer Governing Equation

2.6.1 Continuity Equation

$$\left[\frac{\partial U}{\partial X}+\frac{\partial V}{\partial Y}\right]=0 \tag{2.20}$$

2.6.2 Momentum Balance Equation

***X* direction:**

Including thermodiffusion

$$\frac{\mathrm{Re}}{\phi}.\left[\frac{\partial U}{\partial \tau}\right]+\frac{1}{Da}.[U]=-\frac{\partial P}{\partial X}+\left[\frac{\partial^2 U}{\partial X^2}+\frac{\partial^2 U}{\partial Y^2}\right] \tag{2.21}$$

***Y* direction:**

Without thermodiffusion

$$\frac{1}{Da}.[V]=-\frac{\partial P}{\partial Y}+\left[\frac{\partial^2 V}{\partial X^2}+\frac{\partial^2 V}{\partial Y^2}\right]-\left[\frac{Ra_{PL}}{\mathrm{Pr}.\mathrm{Re}.Da}\right].(1+\frac{d_2}{d_1})^3.\theta \tag{2.22}$$

Including thermodiffusion

$$\frac{\mathrm{Re}}{\phi}.\left[\frac{\partial V}{\partial \tau}\right]+\frac{1}{Da}[V]=-\frac{\partial P}{\partial Y}+\left[\frac{\partial^2 V}{\partial X^2}+\frac{\partial^2 V}{\partial Y^2}\right]-\left[\frac{1}{\mathrm{Pr}.\mathrm{Re}.Da}\right].(1+\frac{d_2}{d_1})^3.[Ra_{PL}.\theta-Ra_{PC}.C] \tag{2.23}$$

2.6.3 Energy Balance Equation

$$\mathrm{Re}.\mathrm{Pr}.\left[\frac{\partial \theta}{\partial \tau}+U.\frac{\partial \theta}{\partial X}+V.\frac{\partial \theta}{\partial Y}\right]=G.\left[\frac{\partial^2 \theta}{\partial X^2}+\frac{\partial^2 \theta}{\partial Y^2}\right] \tag{2.24}$$

$$\text{Where, } G=\frac{k_e}{k_f}=\frac{\phi.k_f+(1-\phi).k_s}{k_f}=\phi+(1-\phi).\frac{k_s}{k_f} \tag{2.25}$$

Where, k_e is the effective thermal conductivity, k_f is conductivity of the fluid, k_s is the conductivity of the solid and G is the ratio between k_e and k_f.

The definitions of the thermal Raleigh number for the liquid layer Ra_{LL}, solutal Raleigh number for the liquid layer Ra_{LC}, thermal Raleigh number for the porous layer Ra_{PL} and solutal Raleigh number for the porous layer Ra_{PC} are varied depending on the case studied. The same also applies to the definition of the Reynolds number, which is fully derived in Appendix A.

2.6.4 Mass Balance Equation

The mass balance Equation for the species is the same as for the liquid layer.

From Appendix A, the case without thermodiffusion, the Reynolds number is defined as:

$$Re = \sqrt{\frac{Ra_{LL}}{Pr}.\left(1+\frac{d_2}{d_1}\right)^3} \tag{2.26}$$

The above equations also show a clear relationship between the thermal liquid Rayleigh number and the thermal porous Rayleigh number for the case without diffusion and steady state. This derivation is also showed in Appendix A. By assuming that the thickness of the porous layer is approximately that of the entire height of the cavity, this relationship can be expressed as:

$$Ra_{PL} = Ra_{LL}.Da.\left(\frac{d_2}{d_1}\right)^3 \tag{2.27}$$

Each geometrical model also has its own specific boundary conditions depending on the case studied and these are presented next.

2.7 Model Boundary Conditions

In order to analyze the fluid motion properly, the basic conservation laws have to be applied along with the appropriate boundary conditions on each segment of the boundary. In the present case, the cavity is laterally heated and the horizontal temperature gradient is applied parallel to the free surface. The left vertical wall is fixed at a cold temperature T_C, while the right vertical wall is maintained at a hot temperature T_H. The bottom surface is insulated, while the top surface of the liquid cavity has a non-deformable free surface through which heat is lost to the surroundings by natural convection. Since Marangoni convection is studied, the heat loss through the free surface to the surrounding gas is by natural convection. Therefore, the non-dimensional heat flux $Q = Bi.\theta$ is applied, where Bi is the Biot number. The boundary conditions for the four walls of the cavity are presented in Figure 2.2. To take into consideration the Marangoni effect,

which is the variation of surface tension along the free surface, a boundary condition for the shear stress jump along the liquid-gas interface is included. To account for this, a new non-dimensional surface tension is defined as, $\sigma_m = \frac{Ma}{Re.Pr}$. It is a function of the Marangoni number, $Ma = \frac{|\gamma|.\Delta T.L}{\alpha.\mu}$, the Reynolds number *Re*, and the Prandtl number *Pr*, defined previously. For the present experiment, a linear variation of surface tension with temperature is specified at the free surface.

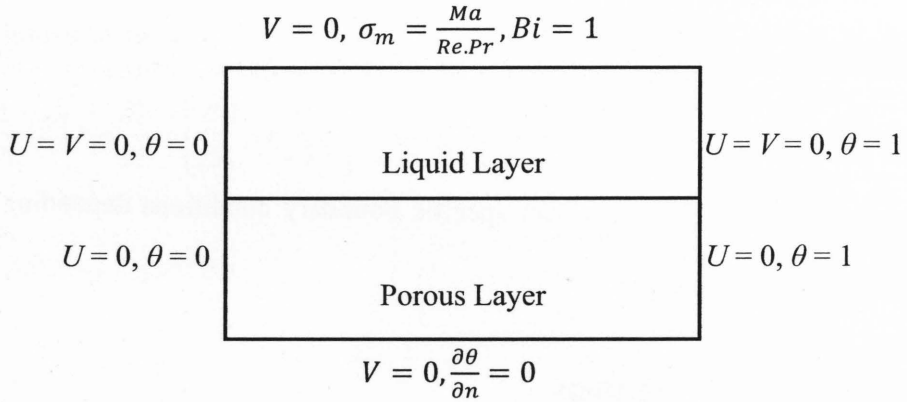

Figure 2.2 Lateral heating boundary condition

2.8 Numerical Solution technique

The fluid dynamic analysis package FIDAP 8.7.0 that uses the finite element method is used in this study. The source code for several cases is outlined in Appendix B. For free surface problems, FIDAP 8.7.0 utilizes the segregated solver. This is an uncoupled method where each degree of freedom is solved seperately. To update the free surface during iteration, the normal stress update algorithm is used for the various cases. In post-processing operations, variables such as the stream function, heat fluxes, flow rates and mass fluxes can be derived from the numerically computed velocity, pressure, temperature and species fields. These capabilites are

provided by the graphs postprocessor programme FIPOST, which can also graphically display the numerical results.

2.8.1 Finite Element Analysis

The numerical procedure consisted of solving the non-dimensional Equations (2.13) to (2.25) using the finite element technique. The finite element technique reduces the infinite number of degrees of freedom in a problem to a finite number by solving a system of equations. For the present two-dimensional model, the computational domain was divided into many small quadrilaterals. To achieve greater accuracy in the results, a finer mesh was applied to the vertical walls of the rectangular cavity and at the free surface where the driving force of the flow is located.

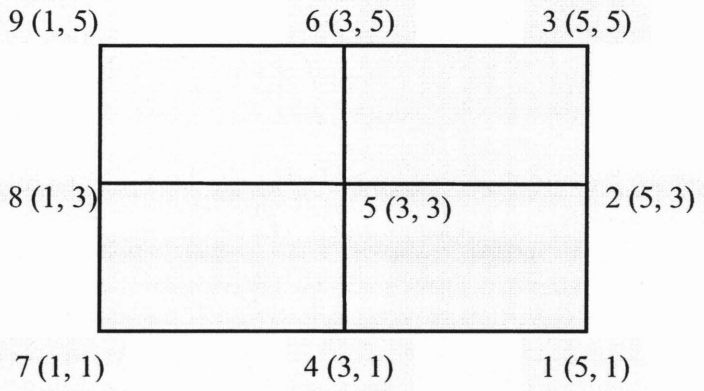

Figure 2.3 Node numbers for key-points

The mesh was defined with a finite number of elements, where the variables were evaluated simultaniously. As can be seen in Figure 2.3, the free surface of the cavity is defined by key-points 3 to 9, and the fluid-porous layer interface by key-points 2 to 8. The velocities, temperature, pressure and species are unknown and are numerically calculated at each node in the meshed cavity. The convergence criterion for the iterative solution of symmetric and non-

symmetric linear equation systems is 1.0E-6. Therefore, the iterations will continue until an error of 1.0E-6 is found between two consecutive iterations.

2.8.2 Mesh Sensitivity Analysis

Performing a mesh sensitivity ananlysis is an integral part of producing accurate, time-efficient and cost-effective results. For this study,we used the same mesh as used by Kozak *et al.* (2004). They used a mesh of 120 elements in the x-axis by 40 elements in the y-axis for the two-dimensional laterally heating conditions. Since a high temperature gradient has been assumed to occur parallel to the free surface, fine nodal spacing near the hot and cold wall, as well as the free surface has been used (figure 2.4).

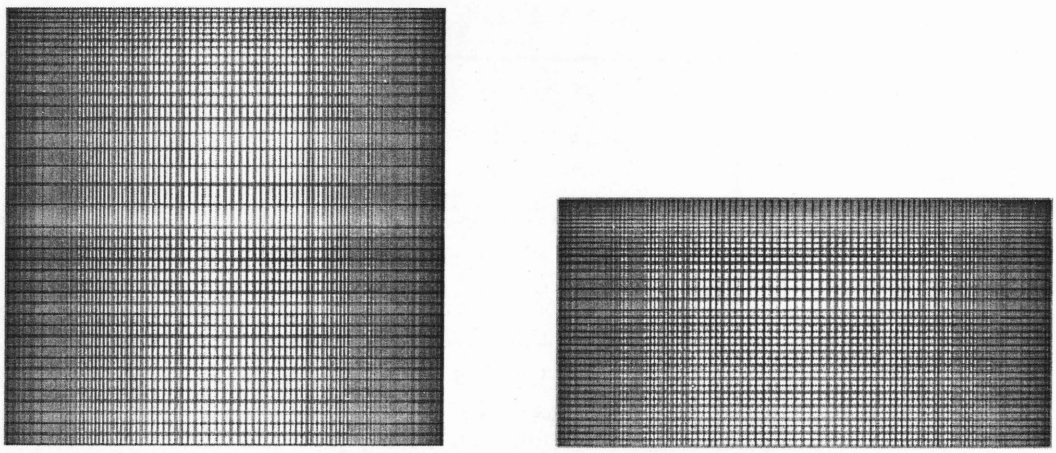

(a) (b)

Figure 2.4 Finite element mesh for model defined by 240 elements in the X-axis by 80 elements in the Y-axis: (a) AR=1, and (b) AR=2

CHAPTER 3

Buoyancy and Marangoni convection

3.1 Introduction

To study the patterns of fluid motion, the discipline of fluid mechanics utilizes several different techniques to visualize the flow. One common type of line pattern is a stream line, which is a line everywhere tangent to the velocity vector at any given instant [35]. In this study, to display the results of computed flow fields for the two-dimensional modeling, stream functions are employed. The stream function Ψ is a clever device that allows us to satisfy the continuity equation and then solve the momentum equation directly for the single variable Ψ. For two-dimensional incompressible flow, the stream function Ψ is determined using the following relationships: $U = \frac{\partial \Psi}{\partial Y}$ and $V = -\frac{\partial \Psi}{\partial X}$. The lines of constant Ψ are the stream line pattern of the flow in the graphical results.

Two different cases are studied in this present chapter. The first case is the buoyancy or gravity driven convection and the second case is the Marangoni or thermocapillary convection with two different fluid mixtures. The fluid mixtures used for the present study are 90% water-10% isopropanol and 50% water-50% isopropanol. To see the effects of the Prandtl number on buoyancy and Marangoni convection, these two different water-isopropanol mixtures has been selected. The physical properties of water-isopropanol mixtures are given in Appendix C. Both the buoyancy and Marangoni convections are studied and compared with each other for two different Rayleigh numbers (calculated from two different temperature differences). To analyze the results, streamline contours, isotherms and velocities at the vertical median of the cavity have

been plotted. To observe the flow phenomena, two different aspect ratios and thickness ratios have been used. From the results, it could be seen whether the flow penetrates in the porous layer or not. The results are compared to the similar analysis by Saghir *et al.* (2005) and Kozak *et al.* (2004).

3.2 Convection in the presence of Buoyancy

The main accelerating factor for buoyancy convection is the gravity force. For a liquid having density differences $\Delta\rho_f$, arising from temperature or concentration differences, the gravitational body force (or buoyancy force) $g.\Delta\rho_f$ will drive the motion. In the present analysis, concentration difference is not taken into consideration. As the buoyancy convection is directly proportional to the Rayleigh numbers, we use two different Rayleigh numbers (for $\Delta T = 5$ and $\Delta T = 10$). Also, to observe the effect of Prandtl number on the buoyancy convection, two different water-isopropanol mixtures having different Prandtl numbers has been selected. For the simulation, heat transfer from the free surface has been allowed by using the non-dimensional heat flux equation $Q = Bi.\theta$, where Bi is the Biot number and $Bi = 1$ has been kept for the entire analysis.

3.2.1 Various effects on Buoyancy Convection

From the linear stability analysis performed by Saghir *et al.* (2005), Kozak *et al.* (2004), and Desaive *et al.* (2001), as the fluid layer thickness decreases, the flow penetrates into the porous layer. Figure 3.1 shows streamlines of buoyancy convection for two different aspect ratios and thickness ratios with the thermal liquid Rayleigh number held constant at Ra_{LL}=8.29E04. When d is set to 0.50, the flow remains in the liquid layer for both $AR = 1$ and 2 and the porous layer acts simply as a rigid wall barrier preventing the flow from protruding in the porous cavity (figure

3.1a). When d =0.90, the flow dominates the porous layer of the cavity with the cell now within the porous layer itself (figure 3.1b). For both the thickness ratios, it is clear that the maximum streamline values increase as the aspect ratio increases from AR = 1 to AR = 2. The reason behind it is that, as the aspect ratio increases, the liquid gets more space to move and also the gravitational force becomes more active. However, as the thickness ratio increases, the streamline values decrease. The reason behind it is that, as the thickness ratio increases, the liquid gets less space to move and also the gravitational force becomes less effective.

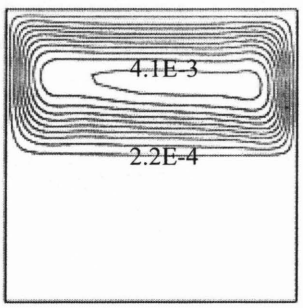

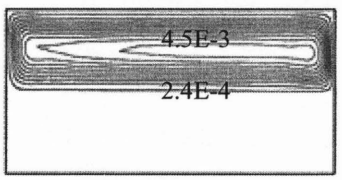

$\Delta\Psi$ = 4.29E-4 $\Delta\Psi$ = 4.73E-4

(a) d = 0.50

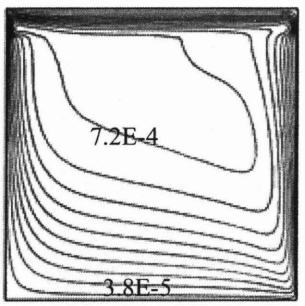

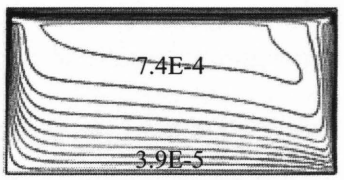

$\Delta\Psi$ = 7.61E-5 $\Delta\Psi$ = 7.82E-5

(b) d = 0.90

AR = 1 AR = 2

Figure 3.1 Streamlines for the buoyancy convection (Pr = 10.85, Ra_{LL} = 8.29E04, Ma = 1)

Figure 3.2 represents the isotherms for two different aspect ratios and thickness ratios. From this figure, it can be easily seen that, for all the cases, the isotherms in the liquid layers are strongly distorted and locally there exists negative horizontal temperature gradients, $\frac{\partial T}{\partial x}$ due to the presence of natural convection in the liquid layer.

As predicted earlier from the linear stability analysis by Kandaswamy and Eswaramurthi (2008), the convective heat transfer rate goes down and the motion of the fluid particles becomes lower as the Darcy number in the porous layer decreases. So, as in our case the Darcy number is 1.0E-05, the heat transfer in the porous layer takes place by the mode of conduction. For thickness ratio d = 0.50, the corresponding isotherms are slightly distorted from their vertical position (figure 3.2a). So, the convective fluid flow or motion is present in the porous layer. However, the flow is very weak and the heat transfer takes place as a conductive mode. But as the thickness ratio increases, the buoyancy-driven convection dominates in the porous layer and the isotherms are strongly distorted from their vertical positions (figure 3.2b). That reflects the presence of strong convective flow in the porous layer. For all the cases, a large temperature gradient exists both near the cold (left) and the hot (right) wall.

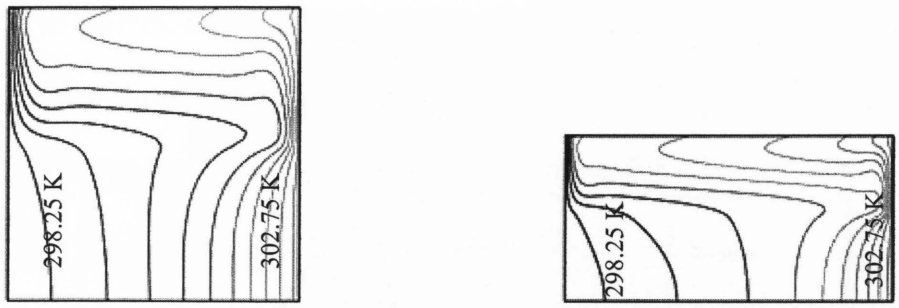

(a) $d = 0.50$

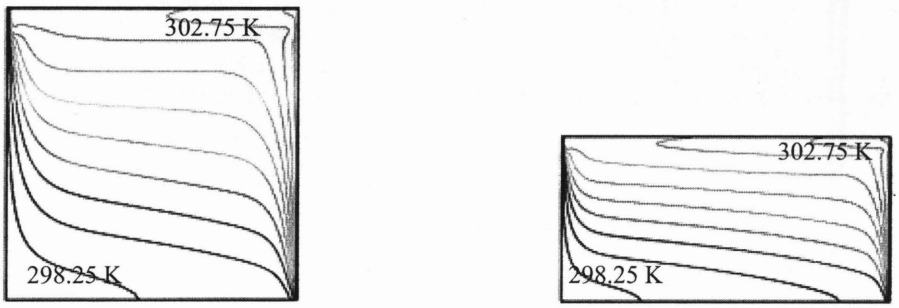

(b) $d = 0.90$

$AR = 1$ $AR = 2$

Figure 3.2 Temperature contours for the buoyancy convection

($Pr = 10.85$, $Ra_{LL} = 8.29e04$, $Ma = 1$)

Figure 3.3 shows the comparison of velocities for two thermal Rayleigh numbers having same Prandtl number 10.85 and thickness ratio 0.50. From these figures we can see that for the both AR = 1 and 2, the velocity increases with increasing the thermal Rayleigh number. For all the cases, we can clearly observe that the velocity is deformed in the liquid layer. This indicates the presence of convective flow in the liquid layers. Also we can easily realize that for all the cases a single cell rotating in the counter clockwise direction is present in the liquid layer. The shape of

the velocity profiles remains same for both thermal Rayleigh numbers. For all the cases a very weak convective flow is observed in the porous layer.

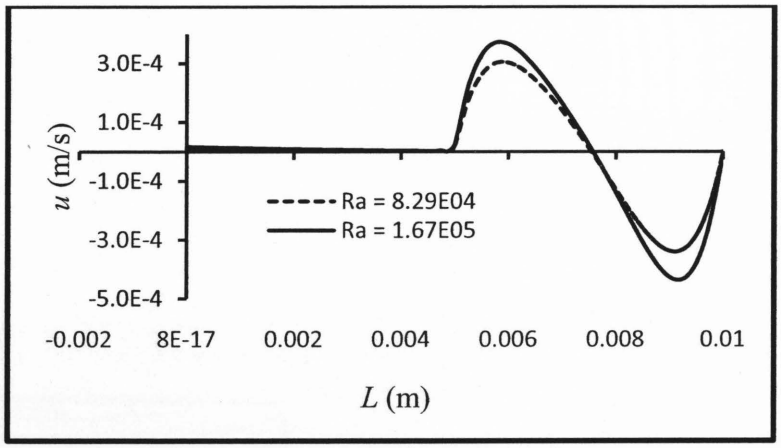

(a) $AR = 1$

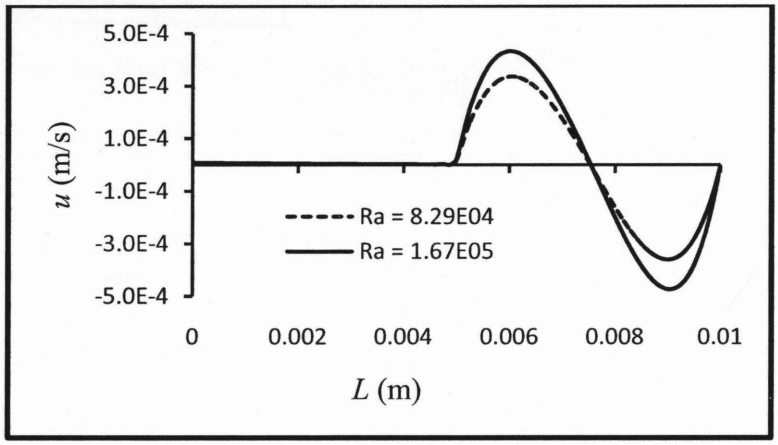

(b) $AR = 2$

Figure 3.3 Effects of thermal Rayleigh number

Figure 3.4 represents the effect of Prandtl number on velocity profiles. We plot velocities for two different water-isopropanol mixtures having same temperature difference ($\Delta T = 5$) and same thickness ratio ($d = 0.50$). One of the using liquids is 90% water-10% isopropanol having Prandtl

number of 10.85 and another one is 50% water-50% isopropanol having Prandtl number of 49.17. From the figure we can see that velocity decreases with increasing Prandtl number. The reason behind it is that the liquid having Prandtl number 10.85 has higher thermal conductivity than the liquid having Prandtl number 49.17 [Appendix C].

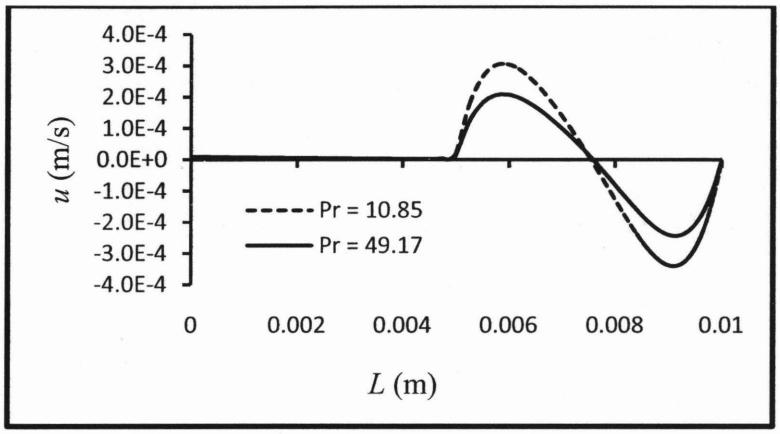

(a) $AR = 1$

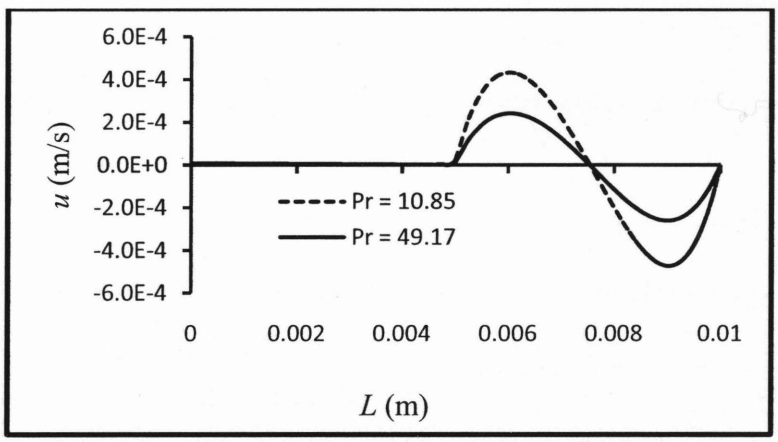

(b) $AR = 2$

Figure 3.4 Effects of Prandtl number

3.3 Convection in the presence of Marangoni

The Marangoni effect (also called Gibbs-Marangoni effect) is the convection in a liquid layer due to the surface tension differences. Since a liquid with a high surface tension pulls more strongly on the surrounding liquid than one with a low surface tension, the presence of a gradient in surface tension will naturally cause the liquid to flow away from regions of low surface tension. The surface tension gradient can in turn be caused by concentration gradient or by a temperature gradient. For our present analysis only temperature gradient is taken into consideration and two different Marangoni numbers (calculated for ΔT = 5 and 10) are used. Marangoni effect is important for the convections in micro-gravity conditions. So we use microgravity condition (g = 10E-5.g_o) to investigate the Marangoni convection. We calculated non-dimensional Marangoni numbers by using coefficient of surface tension for water-isopropanol mixtures [36].

3.3.1 Various effects on Marangoni Convection

Figure 3.5 represents the streamlines of thermocapillary convection for two different aspect ratios and thickness ratios. From this figure we can see that for the thickness ratio d = 0.50 the flow is limited to the liquid layer only (figure 3.5a). The porous layer acts as a solid wall and the flow remains only in the liquid layer. When the thickness ratio d is set to 0.90, the flow becomes partially dominant in the porous layer for both AR = 1 and 2 (figure 3.5b). Also, we can see that the streamline values get weaker as the aspect ratio increases. However, in the case of buoyancy convection, streamline values get stronger as the aspect ratio increases (figure 3.1). We can also see that the flow gets weaker when the thickness ratio d increases. This is the same as for buoyancy convection (figure 3.1). It is also noted that, for all the cases, the center of the

convective cell appears close to the free surface and hot side wall. This is due to the presence of the surface tension force at the free surface and the steep temperature gradient near the hot wall.

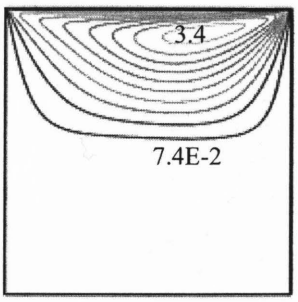

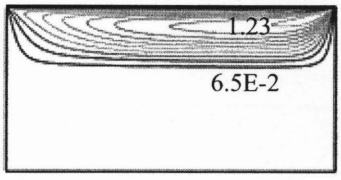

$\Delta\Psi = 1.47\text{E-}1$ $\Delta\Psi = 1.26\text{E-}1$

(a) $d = 0.50$

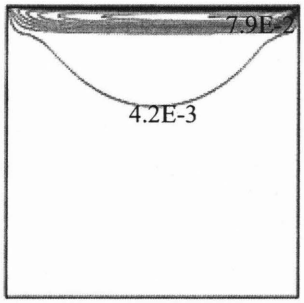

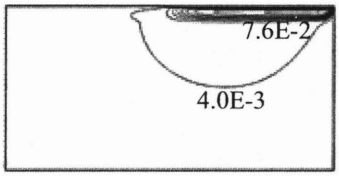

$\Delta\Psi = 8.3\text{E-}3$ $\Delta\Psi = 8.0\text{E-}3$

(b) $d = 0.90$

$AR = 1$ $AR = 2$

Figure 3.5 Streamlines for Marangoni convection ($Pr = 10.85$, $Ra_{LL} = 0.829$, $Ma = 2.21\text{E}4$)

The isotherms for different aspect ratios and thickness ratios are shown in figure 3.6. As in the buoyancy convection (figure 3.2), the isotherms in the liquid layer are strongly distorted and, locally, there exists negative horizontal temperature gradients. That is due to the presence of thermocapillary convection in the liquid layer. For both thickness ratios d (even for $d = 0.90$), the

corresponding isotherms in the porous layer are distorted from their vertical positions. But if we compare with figure 3.2, we can see that the distortions of the isotherms in the porous layer are less than from the buoyancy convection. Also, we can see that, as the thickness ratio d increases, isotherms move towards the cold wall. That indicates, as the thickness ratio increases, convective flow dominates more into the porous layer.

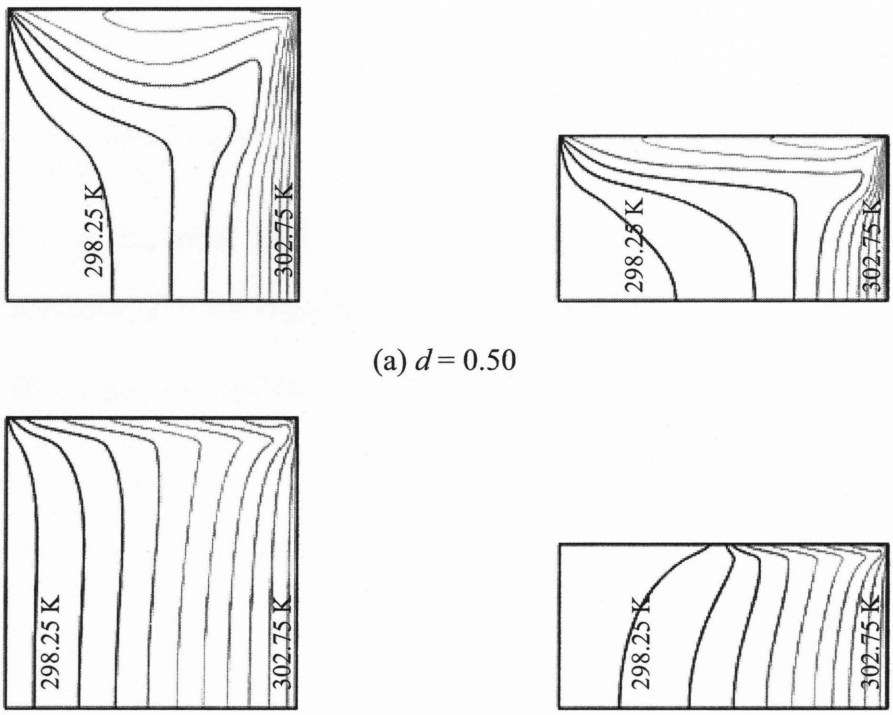

(a) $d = 0.50$

(b) $d = 0.90$

$AR = 1$ $AR = 2$

Figure 3.6 Temperature contours for Marangoni convection

($Pr = 10.85$, $Ra_{LL} = 0.829$, $Ma = 2.21E4$)

Figure 3.7 represents the difference in velocities for the buoyancy and the Marangoni convection. From this figure, we can see that the buoyancy convection is stronger than the

Marangoni convection. Since strong gravity force dominates the buoyancy convection, convection becomes very strong. However, a mimic microgravity condition is considered for the Marangoni convection, so convection becomes too weak to be noticed due to the absence of buoyancy. From the figure, we can also observe that the velocity in the free surface is zero for the buoyancy convection but non-zero for the Marangoni convection. The reason behind it is that, at the free surface, we applied the no slip boundary condition for the buoyancy convection. And for the Marangoni convection, we consider the upper surface as a free surface.

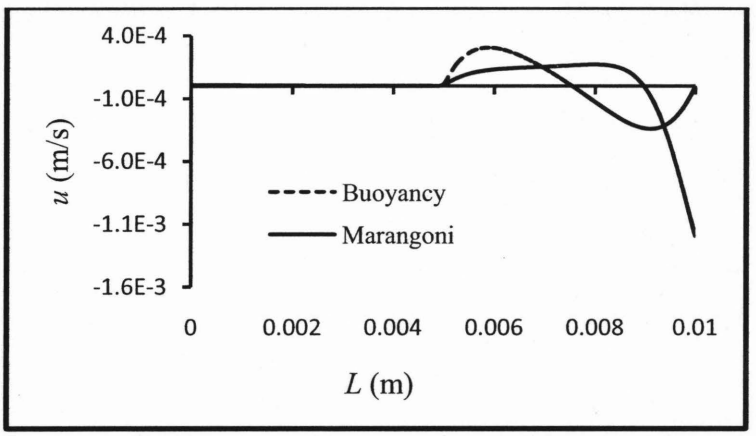

(a) $AR = 1$

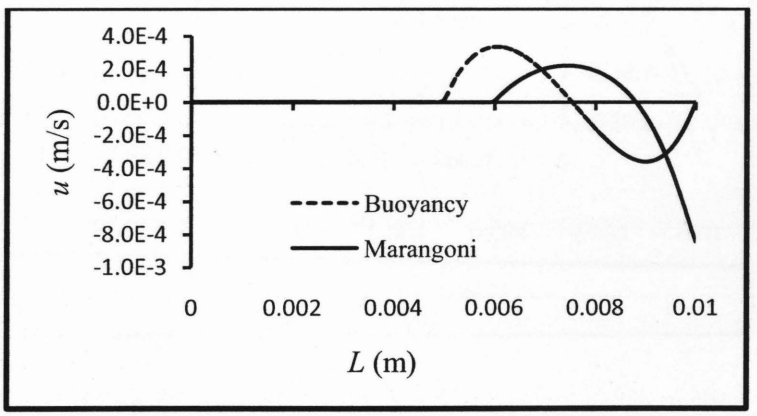

(b) $AR = 2$

Figure 3.7 Comparison between the buoyancy and the Marangoni convection ($Pr = 10.85$)

Figure 3.8 represents the effect of changing the Marangoni number for the same liquid having the same Prandtl number. From this figure, we can easily observe that convective flow increases with increasing Marangoni number. From figure 3.8a, we can also see that the velocity variation due to the change of Marangoni number for aspect ratio $AR = 1$ is very small. However, figure 3.8b shows that the velocity for $AR = 2$ is very sensitive to the Marangoni number.

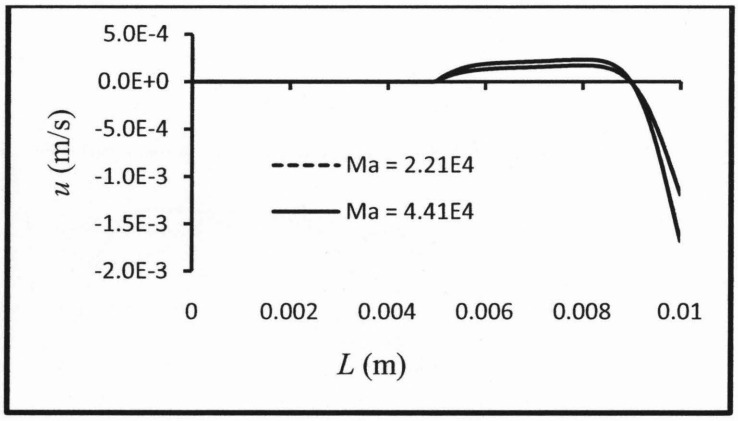

(a) $AR = 1$

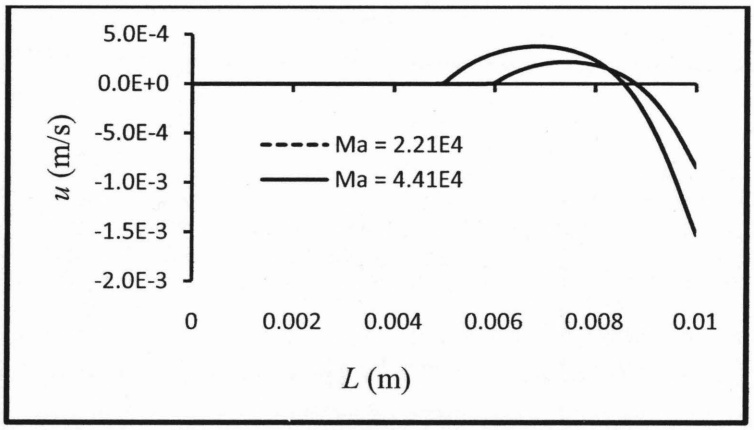

(b) $AR = 2$

Figure 3.8 Effect of Marangoni number ($Pr = 10.85$, $d = 0.50$)

Figure 3.9 shows the velocity profiles of two different Prandtl numbers for the same temperature difference and thickness ratio. Two different water-isopropanol mixtures having Prandtl numbers 10.85 and 49.17 are used for this analysis. From this figure, we can easily realize that, for the both AR = 1 and 2, the convective flow becomes weaker with increasing Prandtl number. The same scenario happened for the buoyancy convection as well (figure 3.4).

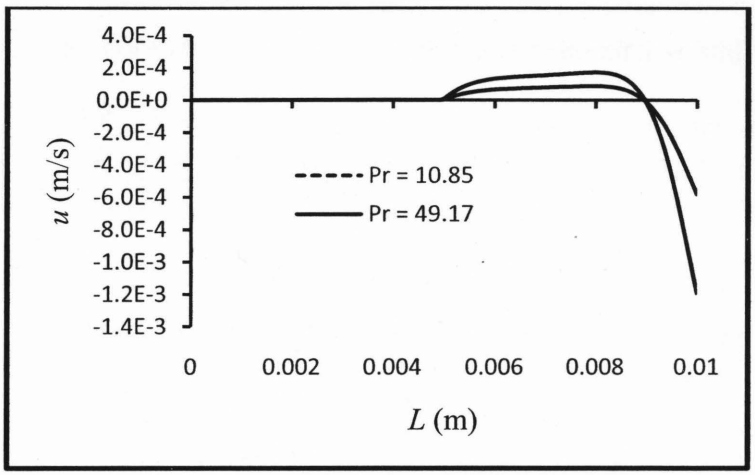

(a) $AR = 1$

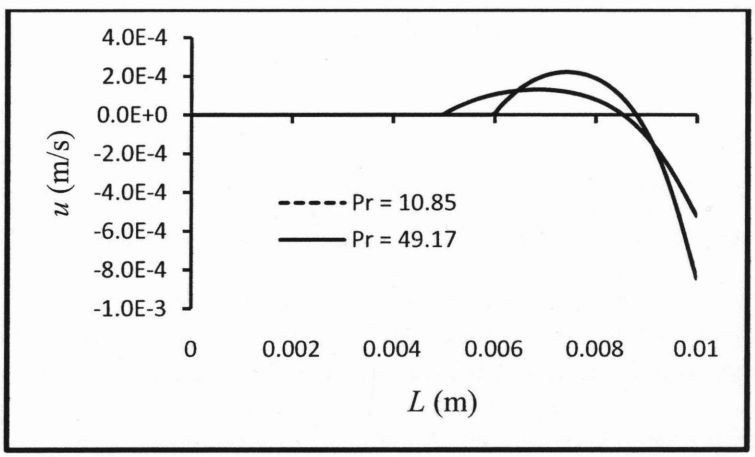

(b) $AR = 2$

Figure 3.9 Effect of Prandtl number ($d = 0.50$, $\Delta T = 5$)

3.4 Summary

In this chapter, the buoyancy and Marangoni convections with different aspect ratios and thickness ratios are studied in detail for two different water-isopropanol mixtures having different Prandtl numbers. From the results, it has been found that the buoyancy convection is stronger than the Marangoni convection. For the buoyancy convection, both the aspect ratio and thickness ratio determine whether the flow dominates in the porous layer or not. As the thickness ratio increases, flow penetrates deeper into the porous layer. Also, for the buoyancy convection, the convective flow increases with increasing Rayleigh number and decreases with increasing Prandtl number. For the Marangoni convection, it has been confirmed that the effects of aspect ratio and thickness ratio on the convective flow are negligible. Convective flow increases with increasing Marangoni number and decreases with the Prandtl number.

CHAPTER 4

Thermo-Solutal Convection in the Presence of Thermodiffusion

4.1 Introduction

In the previous chapter, the mass balance equation was not considered. In the present chapter, we are going to study the thermo-solutal convection by taking into account diffusion (both molecular and thermal) in the mass balance equation.

This chapter has been divided into two major parts. First, molecular diffusion has been applied in the model and the importance of thermo-solutal convection for both the buoyancy and the Marangoni cases has been observed. In the second part, thermodiffusion has been added in the model and how thermodiffusion affects the thermo-solutal convection, has been seen. To activate thermodiffusion, both the molecular diffusion coefficient D_M and the thermodiffusion coefficient D_T in the mass balance equation have been taken into consideration. Both D_T and D_M are assumed as a constant. For the entire calculation, we consider the temperature difference $\Delta T = 5$ and the aspect ratio $AR = 1$.

4.2 Thermo-solutal Convection

As noted by Saghir *et al.* (1998), when heat and species transfer exist within a fluid layer, the temperature and concentration gradients create a convection mode. An equal mass flux at the liquid-porous interface has been assumed. The model with all the boundary conditions used for the study of thermo-solutal convection is given in figure 4.1. For the analysis of thermo-solutal convection, the thickness ratio $d = 0.50$ has been considered.

To see the effects of thermo-solutal convection with respect to time, the transient condition has been used. The term transient means that the simulations are time dependent. To solve the problems in FIDAP in the transient condition, we used the backward Euler time integration method with a variable time increment option. The first 5 time steps has been kept as fixed with a time step increment dt = 1.0E-6s. After 5 time steps, the calculation switches from the fixed time increment method to the variable time increment method.

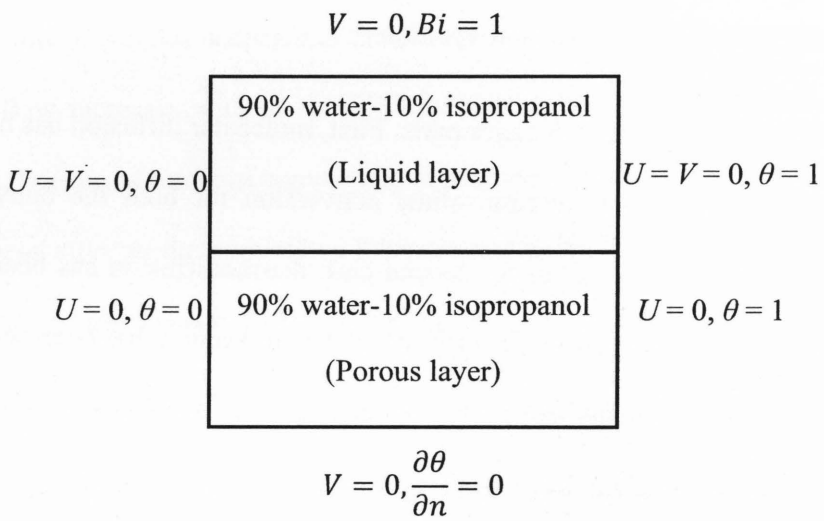

Figure 4.1 Model descriptions with boundary conditions

4.2.1 Buoyancy Convection Condition

To investigate the effects of gravity on thermo-solutal convection, the earth gravity condition is used. As noted by Benano-Melly *et al.* (2001), in some cases, the solutal Rayleigh number Ra_{LC} can be so high that instead of the thermal buoyancy force, the solutal buoyancy force becomes dominant. Then convective flow can change direction or multiple-roll configurations can appear.

Figure 4.2 represents the streamlines and temperature contours for the time step t = 975.6s. Figure 4.2a shows the streamlines for the case with 90% water-10% isopropanol in the entire cavity. For this case, the calculated thermal Rayleigh number Ra_{LL} is 1.036E4 and solutal Rayleigh number Ra_{LC} = 9.36E5. As in the present case $Ra_{LC} > Ra_{LL}$, multicells appear in the liquid layer. We can also see that the flow in the porous layer is not negligible but too weak as compared to the flow in the liquid layer. The reason is that the molecules in the porous layer can't diffuse as fast due to friction with porous particles. Figure 4.2b represents the temperature contours for the time step t = 975.6s. From this figure, it can be clearly observed that the isotherms in the porous layer are slightly distorted from their vertical positions. So the convective flow in the porous layer is not negligible but it is weak. However, the isotherms in the liquid layer for the cases with single liquid are strongly distorted from their vertical positions. That reflects the presence of strong convective flow in the liquid layer.

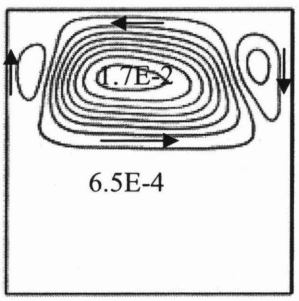

$\Delta\Psi$ = 1.8E-3

(a) Streamlines

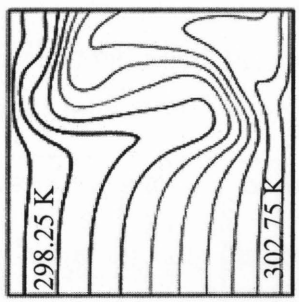

(b) Temperature contours

Figure 4.2 Streamline and temperature contours

4.3 Thermodiffusion

In the previous section, the thermo-solutal convection has been studied. In the present section, the thermo-solutal convection in the presence of thermodiffusion or Soret effect has been studied. The mass flux in a mixture due to a temperature gradient is known as the thermodiffusion or Soret effect. The separation of the components of a mixture subjected to a temperature difference is measured by the Soret coefficient $S_T = D_T/D_M$. For the water-isopropanol binary mixture, the sign of the Soret coefficient is strongly dependent on the concentration. From figure 4.3, it can be seen that the Soret coefficient is positive $S_T > 0$ if the water content is less than 75%, otherwise the Soret coefficient is negative. So, to analyze the effect of thermodiffusion or the Soret effect on thermo-solutal convection, two water-isopropanol mixtures having negative and positive Soret coefficients have been chosen. One of the liquid mixtures is 90% water-10% isopropanol and another one is 50% water-50% isopropanol. Figure 4.3 shows the Soret coefficients for the water-isopropanol binary mixtures.

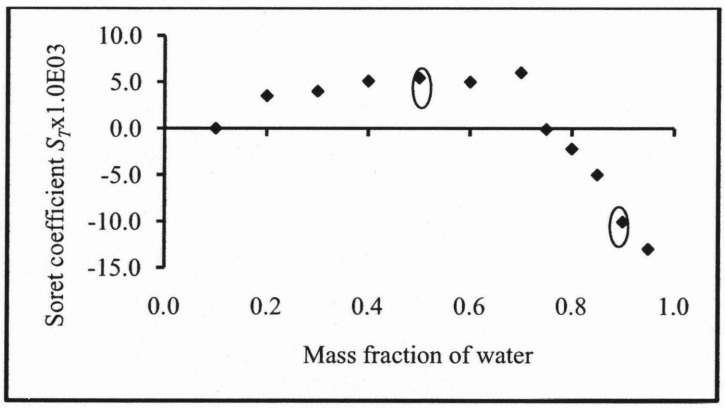

Figure 4.3 Dependence of the Soret coefficient on the mass fraction of water in water-isopropanol mixture (298.15 K) [37]

To activate thermodiffusion, both the molecular diffusion coefficient D_M and the thermodiffusion coefficient D_T in the mass balance equation have been taken into consideration. During the calculation, both D_T and D_M have been assumed to be fixed. From the results, it would be seen how thermodiffusion will create convection without presence of the buoyancy and the surface tension. To minimize the buoyancy effect, a mimic microgravity condition (g = 1.0E-7.g_o) has been used. To see the effects of thermodiffusion on convection with respect to time, the model has been considered as transient in nature. To solve the problem in FIDAP with transient condition, backward Euler time integration method with variable time increment option has been used.

As noted by Jiang *et al.* (2004), when the characteristic time of the convective flow is larger than the characteristic time of the thermal diffusion, then the Soret effect is the dominant force for the composition separation in the cavity and maximum separation is reached when characteristic time is equal to the time of thermal diffusion. From the physical properties of isopropanol we can see that the characteristic time of the thermal diffusion for two water-isopropanol mixtures are 11.49E4s and 55.56E4s (Appendix C). So to analyze the thermodiffusion or Soret effect, we set our calculation end time t_{end} = 5.0E05s. To analyze the Soret effect in details, we analyze two different cases. In the first case, initially 90% water-10% isopropanol is set in the whole cavity. And for the second case, initially 50% water-50% isopropanol is set in the whole cavity. For the entire analysis, we consider a temperature difference of ΔT = 5 and the reference temperature of the cavity is set the average of hot and cold temperature.

4.3.1 Thermodiffusion with negative S_T

In the present analysis, only a single liquid mixture 90% water-10% isopropanol having negative Soret coefficient is used both in the liquid and in the porous layer. The model descriptions and the boundary conditions are given in figure 4.4.

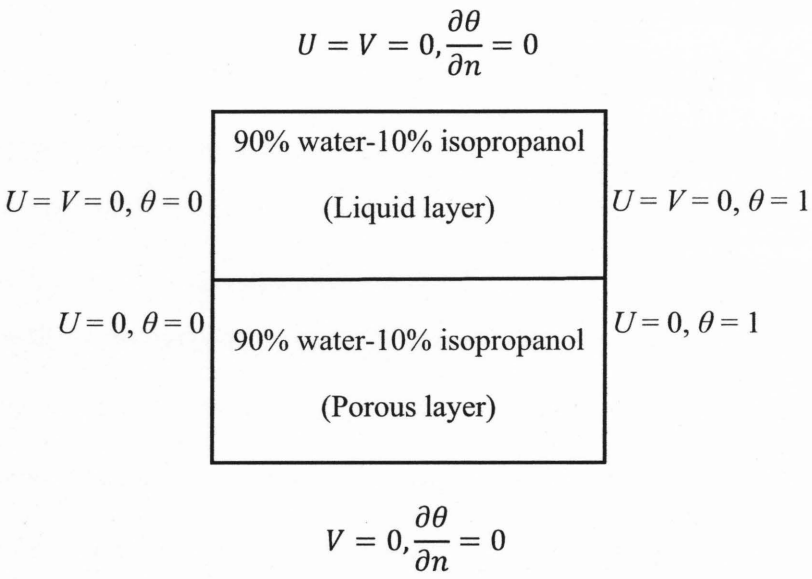

Figure 4.4 Model descriptions and boundary conditions

As mentioned earlier in the literature review (chapter 1), thermodiffusion in a binary mixture have been studied earlier by a lot of researchers. Most of them found that due to the presence of thermodiffusion in a binary mixture, the molecules separate from each other towards the hot and cold walls. If the Soret coefficient of the mixture is negative then lighter component moves towards the hot wall and heavier component moves towards the cold wall. Figure 4.5 shows the streamline contours for different thickness ratios at the time step 500,000s. Figure 4.5a shows the streamlines when the cavity doesn't have any porous medium. From this figure, it can be seen that the streamline values are very weak as compare to the buoyancy and Marangoni

convections. The main reason behind it is that for this analysis microgravity condition (g = 10e-7.g_o) has been considered and the thermocapillary effect has not been considered. Only thermodiffusion effect is considered for this study. As the effect of thermodiffusion on convection is very weak, the maximum and minimum streamline values are very small. Also, the difference between the maximum streamline values and the minimum streamline values are very small. However, as the thickness ratio increases, the convective flow becomes weak. When d is 0.50, the flow remains in the liquid layer only and the flow in the porous layer is negligible (figure 4.5b). When there is no liquid layer (d = 1.0), the convective flow covers the entire cavity. But the flow is very weak compared to the previous cases where the liquid layer exists (figure 4.5c).

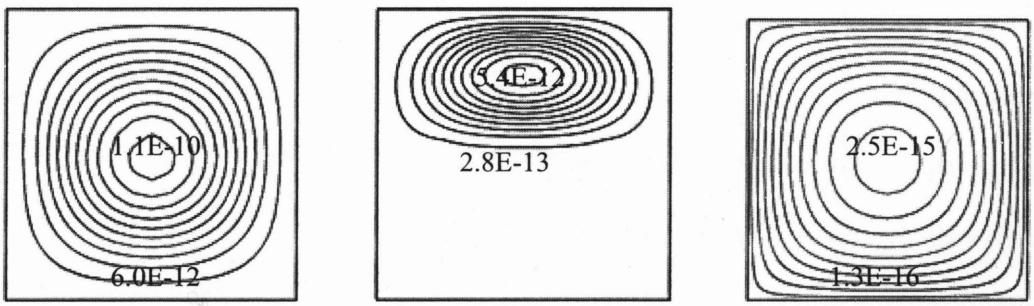

$\Delta\Psi$ = 1.16e-11 $\Delta\Psi$ = 5.69e-13 $\Delta\Psi$ = 2.63e-16

(a) d = 0.0 (b) d = 0.50 (c) d = 1.0

Figure 4.5 Streamline contours

Figure 4.6 shows the temperature contours in the cavity for the time step t = 500,000s. From this figure, it can be seen that for all the thickness ratios, the isotherms are almost vertically parallel. Also the shapes of the isotherms both in the liquid layer and the porous layer are almost the same. That shows very weak convective flow exists in the whole cavity. However, for the

thermo-solutal convection with buoyancy, the isotherms in the liquid layer were strongly distorted from their vertical positions.

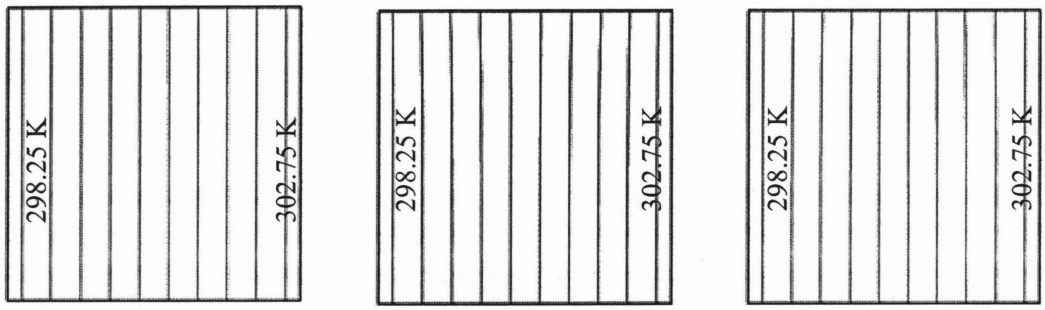

(a) $d = 0.0$ (b) $d = 0.50$ (c) $d = 1.0$

Figure 4.6 Temperature contours

Figure 4.7 represents the isopropanol distributions in the cavity for the thickness ratio $d = 0.50$ only. From this figure, we can see that, as the time increases, the concentration of isopropanol near the hot (right) wall increases. In the same time, the concentration of isopropanol near the cold (left) wall decreases. Due to the presence of thermodiffusion effect, lighter molecules (isopropanol) migrate to the hot wall and heavier molecules (water) migrate to the cold wall. A similar analysis was done by Jiang *et al.* (2004). They found that, in the lateral heating condition, lighter fluid component migrates to the hot side of the cavity. If the concentration along different positions in the cavity has been plotted, it can be easily understood how thermodiffusion affects the isopropanol distributions. Figure 4.8 reflects the isopropanol distribution for different time steps along the horizontal direction of the cavity. From this figure, we can see that, at the initial time step $t = 0$s, both the porous and the liquid layer have the same concentration (0.10). But as the time increases, the concentration near the cold wall (at $H = 0$m) decreases and the concentration near the hot wall (at $H = 0.01$m) increases. For all the time steps, the concentration

varies linearly with distance. At the time t = 500,000s, the isopropanol distribution line appears completely linear.

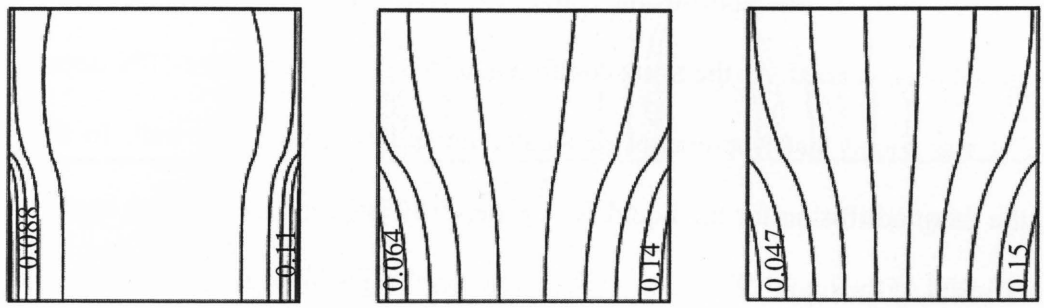

ΔC = 2.4e-3 ΔC = 8.4e-3 ΔC = 1.14e-2

(a) t = 1,000s (b) t = 10,000s (c) t = 500,000s

Figure 4.7 Isopropanol distributions with negative S_T (d = 0.50)

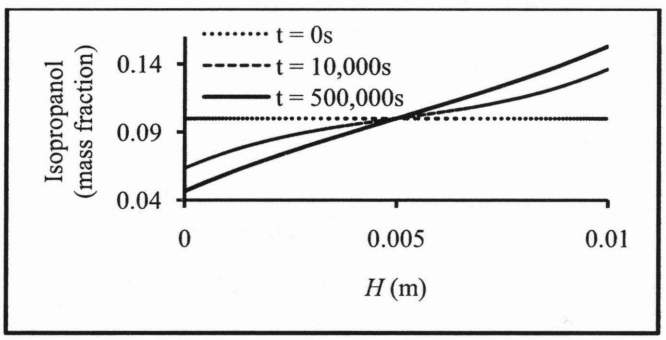

(a) Porous layer (L = 0.003m)

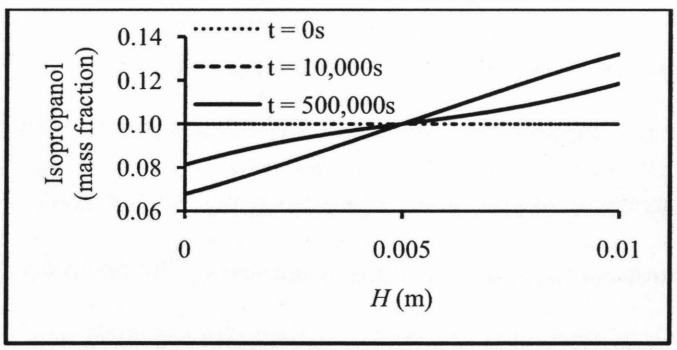

(b) Liquid layer (L = 0.007m)

Figure 4.8 Isopropanol distributions along the horizontal direction of the cavity

4.3.2 Thermodiffusion with Positive S_T

In the previous section, thermodiffusion convection with the liquid having a negative Soret coefficient has been studied. As the Soret coefficient of the liquid 90% water-10% isopropanol is negative, it was found that isopropanol molecules move towards the hot wall. In the present section, the thermodiffusion for the liquid 50% water-50% isopropanol has been examined. The Soret coefficient of the liquid 50% water-50% isopropanol is positive. So, in the present analysis, isopropanol molecules would move towards the cold wall. The model and the boundary conditions used for the present analysis are the same as figure 4.4.

Figure 4.9 shows the isopropanol distributions in the cavity for different time steps. At the beginning (t = 0s), the concentration of isopropanol was uniform everywhere in the cavity. From this figure we can see that as the time increases, the concentration of isopropanol near the hot (right) wall decreases. In the same time the concentration of isopropanol near the cold (left) wall increases. Due to the presence of thermodiffusion effect, lighter molecules (isopropanol) migrate to the cold wall and heavier molecules (water) migrate to the hot wall. If we compare figure 4.9 with the figure 4.7, we can see that two figures have quite opposite behaviours. For the thermodiffusion with liquid 90% water-10% isopropanol, isopropanol component migrates to the hot side wall. But for the thermodiffusion with liquid 50% water-50% isopropanol, isopropanol component migrates to the cold side wall. The reason behind it is that the two liquid mixtures have two different Soret coefficients and Prandtl numbers. The Soret coefficient of 90% water-10% isopropanol is negative. But the Soret coefficient of 50% water-50% isopropanol is positive.

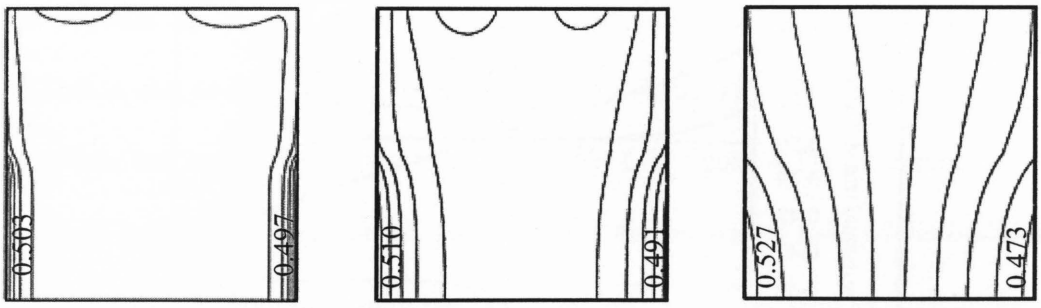

ΔC = 6.67e-4 ΔC = 2.1e-3 ΔC = 6.0e-3

(a) t = 1,000s (b) t = 10,000s (c) t = 500,000s

Figure 4.9 Isopropanol distributions with positive S_T (d = 0.50)

Figure 4.10 shows the isopropanol distribution for different time steps along the horizontal direction of the cavity. From this figure it can be seen that at t = 0s both the porous and the liquid layer have the same concentration (0.50). But as the time increases, the concentration near the cold wall (H = 0m) increases and the concentration near the hot wall (H = 0.01m) decreases. At the time t = 500,000s the isopropanol distribution line appears completely linear. If we compare this figure with figure 4.8, we can easily distinguish the difference of thermodiffusion effect between the liquid mixtures having positive and negative Soret coefficient.

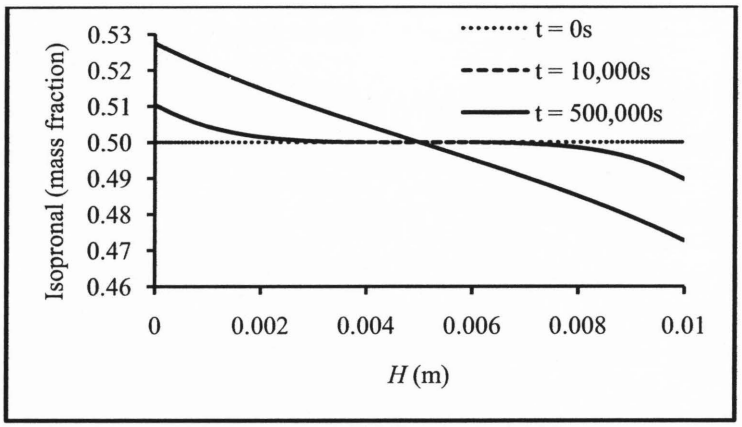

(a) Porous layer (L = 0.003m)

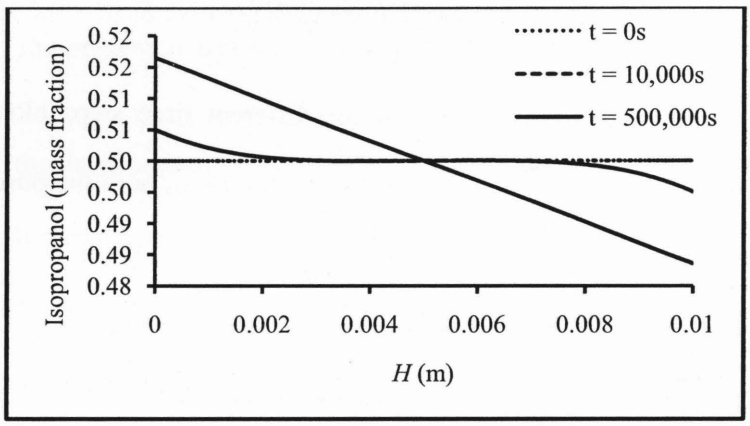

(b) Liquid layer (L = 0.007m)

Figure 4.10 Isopropanol distributions along the horizontal direction of the cavity

4.3.3 Separation ratio

To measure the thermodiffusion effect on binary mixture, the separation ratio is calculated. The separation ratio is a very good device to understand the mass transfer process due to the thermodiffusion convection. Figure 4.11 shows the calculated separation ratios for different porosities at the time step t = 500,000s. From figures 4.11a and 4.11b, it can be seen that the separation ratio decreases with increasing porosity. The reason is, as the porosity increases, the

distances between the porous particles are increased and more liquid exists in the porous medium. Hence, due to the presence of more liquid, the buoyancy force becomes strong in the porous medium and reduces the thermodiffusion effect. If figure 4.11b is compared with the figure 4.11a, it can be seen that, for the same porosity the separation ratio of the liquid mixture having negative S_T is higher than that of the liquid mixture having positive S_T.

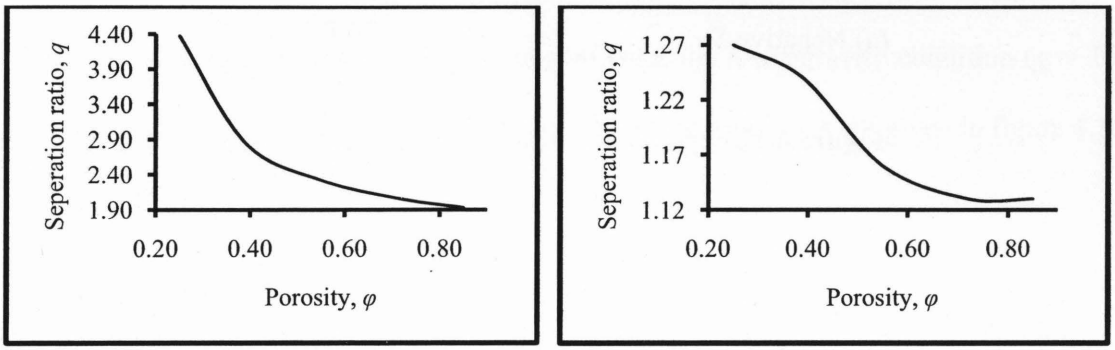

(a) Negative S_T (b) Positive S_T

Figure 4.11 Separation ratios for different porosities

Figure 4.12 shows the effect of gravitational acceleration on thermodiffusion at the time step t = 500,000s. This figure clearly shows that the separation ratio decreases with increasing gravitational acceleration. And the minimum separation appears at the earth gravity condition (g = 9.8m/s^2). As mentioned earlier in the chapter 3, the gravitational force is the main accelerating factor for the buoyancy body force term. So the buoyancy force increases with increasing gravitational acceleration and reduces the thermodiffusion effect. However, the separation ratio of the liquid mixture having negative S_T is more sensitive to the gravitational force than that of the liquid mixture having positive S_T.

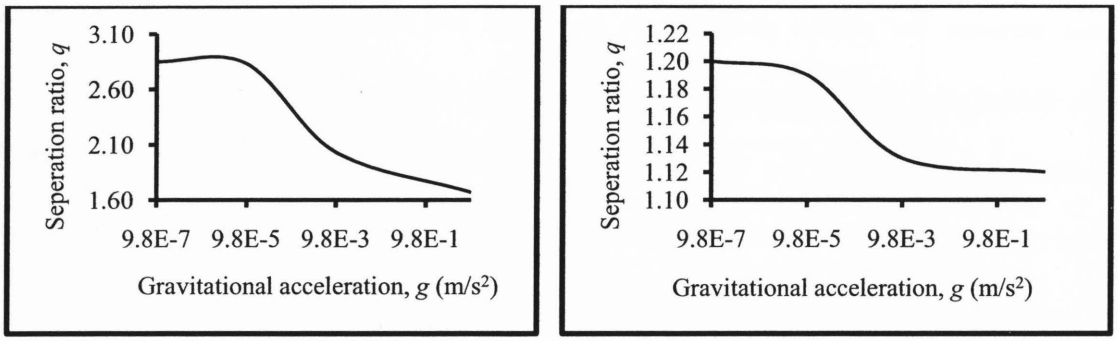

(a) Negative S_T (b) Positive S_T

Figure 4.12 Separation ratios for different gravities

4.4 Thermo-Solutal Convection for Combined Fluid

In the previous two sections, thermo-solutal convection has been studied only for a single liquid mixture. In this section the thermo-solutal convection for combined liquid mixtures would be analyzed. To investigate the effects of gravity and surface tension on thermo-solutal convection, both the buoyancy and the Marangoni convections are studied in detail. For the buoyancy case, the earth gravity condition and, for the Marangoni case, the microgravity condition (g = 1.0E-5.g_o) has been studied. The model description and boundary conditions are given in figure 4.13.

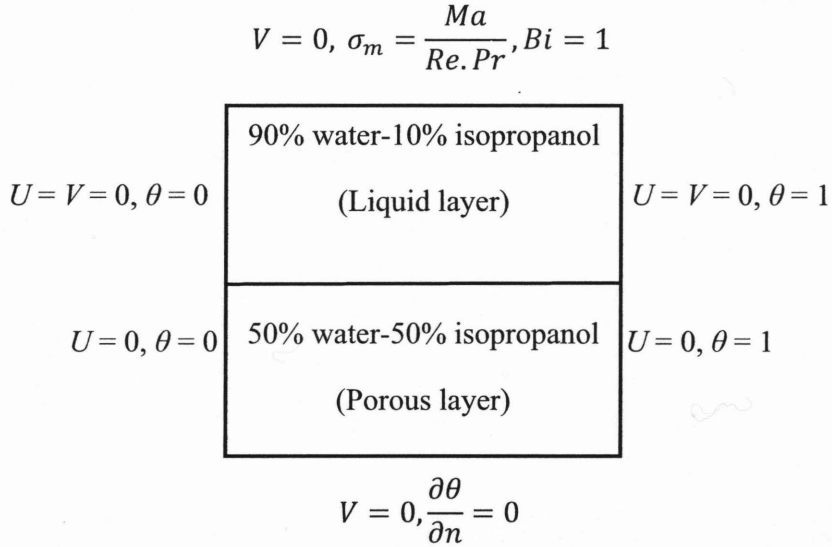

Figure 4.13 Model descriptions with boundary conditions

4.4.1 Buoyancy Convection Condition

Figure 4.14 represents the streamlines and temperature contours for the time step t = 975.6s. Figure 4.14a shows the streamlines for the case when 90% water-10% isopropanol is set in the liquid layer and 50% water-50% isopropanol is set in the porous layer. Due to the presence of two different liquid mixtures having positive and negative solutal expansion coefficients,

multicells appear in the liquid layer and the convective flow becomes weaker than the cases with a single liquid mixture. For all the cases, it can be seen that the flow in the porous layer is not negligible but is weak compared to the flow in the liquid layer. The reason for this is that the molecules in the porous layer can't diffuse so fast due to the friction with porous particles. Figure 4.14b represents the temperature contours for the time step t = 975.6s. From this figure, it can be seen that, for all the cases, the isotherms in the porous layer are slightly distorted from their vertical positions. So the convective flow in the porous layer is not negligible but too weak.

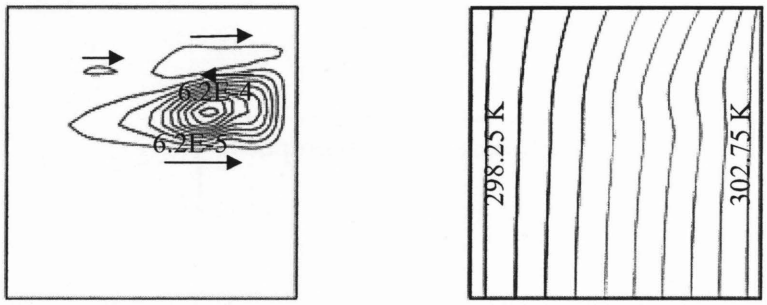

$\Delta\Psi$ = 7.0E-5

(a) Streamlines, (b) Temperature contours

Figure 4.14 Streamline contours

Figure 4.15 represents the isopropanol distributions in the cavity for different time steps. At the beginning of the calculation, the concentration of isopropanol in the porous layer was set to 0.50 and the concentration of isopropanol in the liquid layer was set to 0.10. From this figure, it can be interestingly seen that, as the time increases, the concentration of isopropanol in the liquid layer becomes higher than that of the porous layer. The reason is that the gravitational force accelerates the heavier component (water) in the downward direction of the cavity and hence the lighter component (isopropanol) moves in the upward direction of the cavity. Also, for the time

step t = 975.6s, we can see that the isopropanol distribution in the porous layer is almost linear. But, due to the presence of convective flow in the liquid layer, the concentration lines are nonlinear.

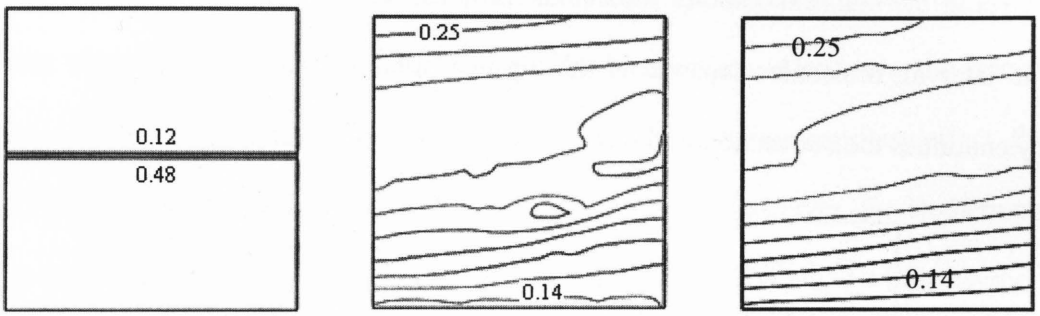

ΔC = 0.04 ΔC = 0.012 ΔC = 0.012

(a) t = 0s (b) t = 406.5s (c) t = 975.6s

Figure 4.15 Isopropanol distributions

Figure 4.16 shows the concentration of isopropanol for various time steps along the vertical median direction of the cavity. From this figure, it can be seen that, at the initial time t = 0s, the porous layer has the constant concentration of 0.50 and the liquid layer has the constant concentration of 0.10. But, as the time increases, the concentration of isopropanol in the porous layer decreases and in the liquid layer increases. As discussed earlier, the reason is that the gravitational force attracts heavier component (water) in downward direction. So as the time increases, water component migrates to the lower portion and isopropanol component migrates to the upper portion of the cavity. It can be also observed that the concentration for the time step t = 162.6s and for the time step t = 975.6s are almost the same. Also, when the time step has been increased further, the concentration remains uniform (not shown in the figure). However, for the liquid with 90% water-10% isopropanol, the calculated thermal characteristic time, τ_{th} is 769.23s

and the diffusive characteristic time, τ_D is 1.15E5s (Appendix C). So to observe the effect of molecular diffusion on thermo-solutal convection, it is needed to continue the calculation up to the time step t = 1.15E5s. But, in the earth gravity condition, due to the presence of strong buoyancy (both thermal and solutal), molecular diffusion can't be effective. So, within a very short time interval, molecules separate in the top and bottom portions of the cavity and only buoyancy continues the convection in the cavity.

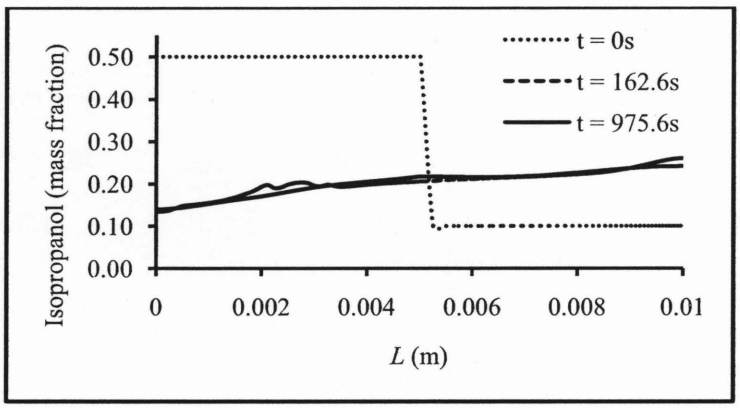

Figure 4.16 Concentration of isopropanol along the vertical median direction

4.4.2 Marangoni Convection Condition

In the previous section, we studied the thermo-solutal convection in the presence of buoyancy. But, due to the presence of the strong buoyancy effect, we couldn't observe the influence of molecular diffusion on thermo-solutal convection. To observe the effects of molecular diffusion and surface tension on thermo-solutal convection, both the microgravity condition and the free upper surface have been considered for the present study. As in this buoyancy case, initially, we set 90% water-10% isopropanol in the liquid layer and 50% water-50% isopropanol in the porous layer. For this case, the calculated Marangoni number Ma = 2.21E4, the thermal Rayleigh number Ra_{LL} = 0.1036 and the solutal Rayleigh number Ra_{LC} = 9.365.

Figure 4.17 shows the streamlines and isotherms for the time step t = 25,641s. From figure 4.17a, it can be seen that the flow does not exist in the porous layer. The flow remains in the liquid layer only and the porous layer simply acts as a wall. However, for the buoyancy case the centre of the vortex was near to the hot wall and multicells were appeared (figure 4.14a). But for the Marangoni case, the centre of the vortex is near the free surface. Also, near the free surface, streamlines are congested. These are due to the presence of the thermo capillary effect. From the figure 4.17b, we can see that both in the liquid layer and the porous layer, the isotherms are not vertically parallel. That reflects the presence of weak convective flow in the whole cavity. But, in the liquid layer, the isotherms are strongly distorted. However, the isotherms in the porous layer are weakly distorted from their vertical positions. Also, in the liquid layer, the isotherms are congested both near the hot and cold walls. So it can be said that the flow inside the porous layer is very weak as compared to the liquid layer.

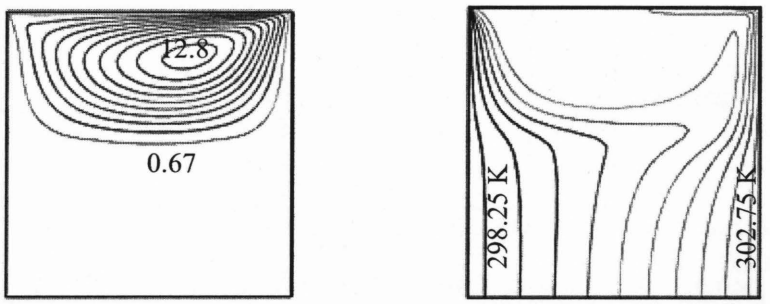

(a) Streamlines (b) Temperature contours

Figure 4.17 Streamlines and temperature contours

Figure 4.18 shows the isopropanol distributions for various time steps in the cavity. From this figure, it can be easily seen that at the early time step, the porous layer has higher concentration than that of liquid layer (figure 4.18a). But, as the time increases, the difference in concentration

between the liquid layer and the porous layer decreases (figure 4.18b). At the time t = 25,641s (which is less than the calculated diffusive characteristic time τ_D = 115,000s), the concentration of isopropanol becomes uniform in the whole cavity (figure 4.18c). If we compare figure 4.18 with the buoyancy case (figure 4.15), we can see that, for the Marangoni case, the two different water-isopropanol mixtures diffuse more slowly than for the buoyancy case. Also, for the Marangoni case, the difference in concentration with respect to time decreases slowly. However for the buoyancy case, instead of mixing the isopropanol component goes into upper portion and the water component goes into the bottom portion of the cavity. The main reason is that, for the buoyancy case, the strong gravitational force was effective but, for the Marangoni case, the gravitational force is not negligible but too weak, so it doesn't have a strong effect on the molecular movements.

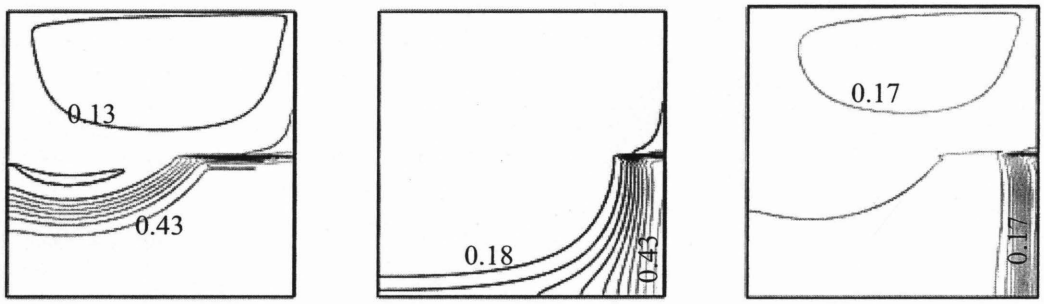

(a) t = 769.2s (b) t = 7,692.3s (c) t = 25,641s

Figure 4.18 Isopropanol distributions

Figure 4.19 shows the concentration of isopropanol for various time steps along the vertical median direction of the cavity. From this figure, we can clearly see that, initially (t = 0s), the porous layer has the concentration of 0.50 and the liquid layer has the concentration of 0.10. Then it can be seen that the concentration of isopropanol gradually decreases with increasing

time steps. And, at the time step t = 25,641s, the concentration of isopropanol becomes uniform in the whole cavity. But this time step is not more than the diffusive characteristic time τ_D = 115,000s. As the upper surface is assumed to be free, the Marangoni or thermocapillary effect influences on thermo-solutal convection. So, before reaching the diffusive characteristic time, the water and isopropanol components are completely mixed together and create a uniform water-isopropanol mixture of concentration (isopropanol) 0.17.

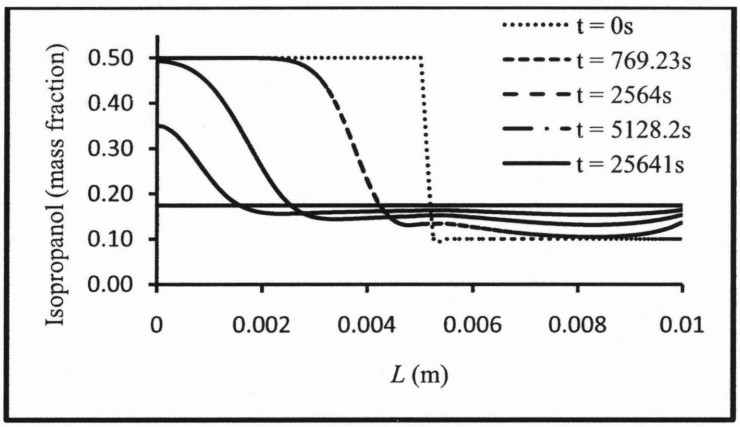

Figure 4.19 Concentration of isopropanol along the vertical median direction

Figure 4.20 shows the comparison of isopropanol distribution between the buoyancy and the Marangoni convection at the time step t = 769.23s. From this figure, we can see that, for the buoyancy convection, the water and isopropanol components are mixed in the whole cavity. However, for the Marangoni convection, the concentration of isopropanol in the porous layer is almost 0.50 and in the liquid layer is almost 0.10. So it is clear that, for the Marangoni case, the isopropanol components diffuse very slowly with respect to time. However, for the buoyancy case, isopropanol components diffuse strongly within a very short time step.

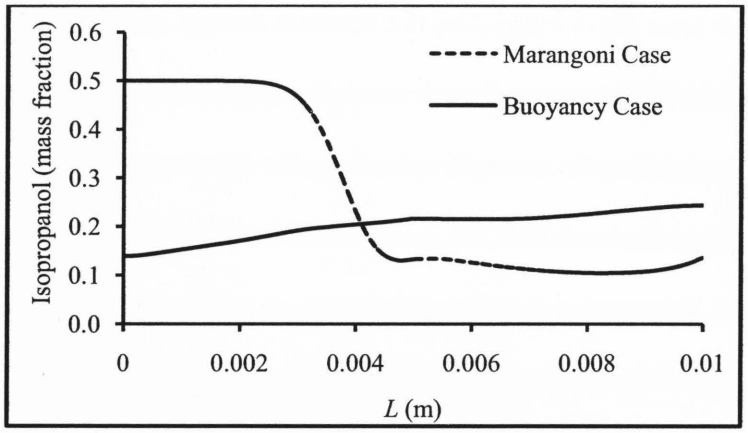

Figure 4.20 Comparison between the buoyancy and the Marangoni case

4.5 Thermodiffusion Effect for Combined Fluid

In the previous section (section 4.3), it has been studied thermodiffusion convections for single liquid mixtures. From the results, it has been found that, for the liquid mixture having a negative Soret coefficient, the isopropanol component moves towards the hot wall. However, for the liquid mixture having a positive Soret coefficient, the isopropanol component moves towards the cold wall. Now we are interested to see what will happen if we use two different liquid mixtures (both negative and positive Soret coefficients) in the same model. To analyze this case, initially, 90% water-10% isopropanol has been set in the liquid layer and 50% water-50% isopropanol has been set in the porous layer. The model including boundary conditions is shown in figure 4.21. The solution methods for FIDAP are kept the same as the thermo-solutal convection with combined fluid.

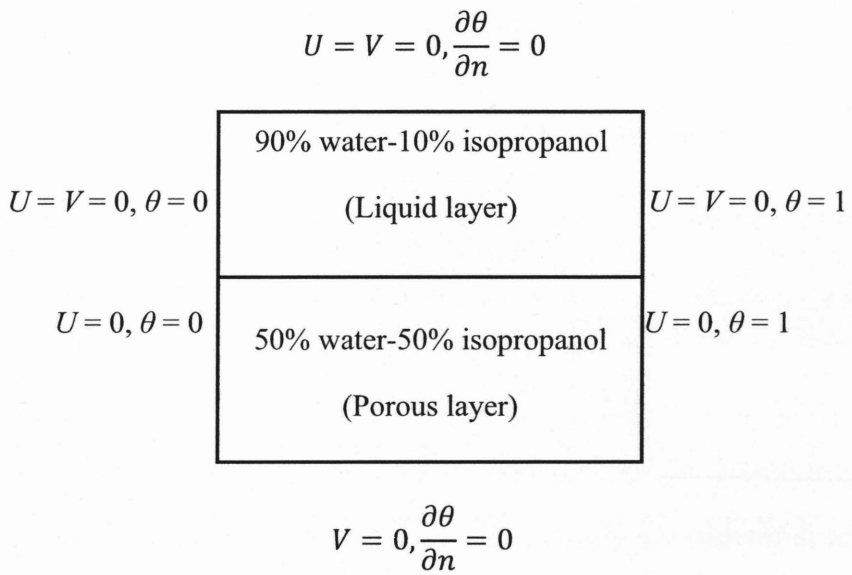

Figure 4.21 Model descriptions and boundary conditions for thermodiffusion

Figure 4.22 shows the streamline contours for different time steps. From this figure, we can see that the streamlines are quite different from the cases with single liquid mixtures. In the early time step, three cells appear in the liquid layer. Two cells are rotating in the clockwise direction and the other cell in the middle is rotating in the counter-clockwise direction (figure 4.22a). But, as the time increases, flow directions of the rolls are changed (figure 4.22b). The reason behind it is that, as the present model has two different mass fractions, with respect to time these two liquids mix together due to the molecular diffusion. At the same time, due to the thermodiffusion effect, isopropanol molecules in the liquid layer move towards the hot wall (due to the negative S_T) and isopropanol molecules in the porous layer move towards the cold wall (due to the positive S_T). When the time increases further at t = 5.0E05s, it can be seen that only a single cell having flow in the clockwise direction appears in the liquid layer (figure 4.22c). As this time step is more than the diffusive characteristic time (τ_D = 1.15E05s), thermodiffusion is now completely effective. We can also see that for, all the time steps, the streamline values are too weak to penetrate into the porous layer.

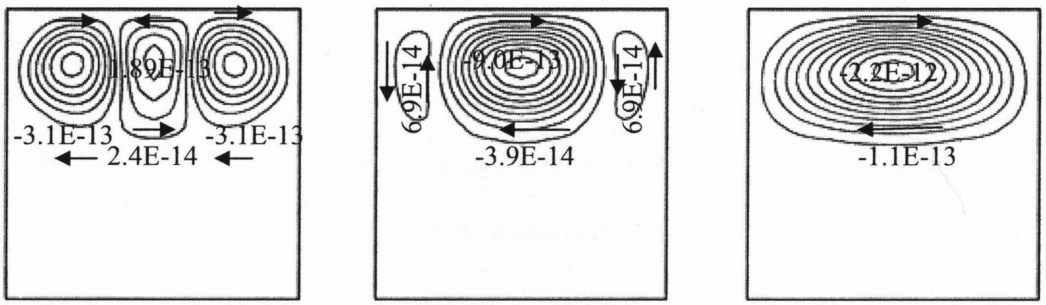

$\Delta\Psi$ = 5.48e-14 | $\Delta\Psi$ = 1.08e-13 | $\Delta\Psi$ = 2.23e-13

(a) t = 2,000s | (b) t = 10,000s | (c) t = 500,000s

Figure 4.22 Streamline contours

To see the nature of the convective flow due to the thermodiffusion, we plot the horizontal component of velocity in the vertical median direction of the cavity. From figure 4.23, we can easily see that, for all the time steps, the flow in the porous layer is too weak. For the time t = 2,000s, a very weak counter-clockwise direction flow exists in the liquid layer. But, for the time t = 10,000s, stronger clockwise direction convective flow exists in the liquid layer. As the time increases further, it can be seen that, at t = 500,000s, the convective flow in the liquid layer becomes strong due to the thermodiffusion effect.

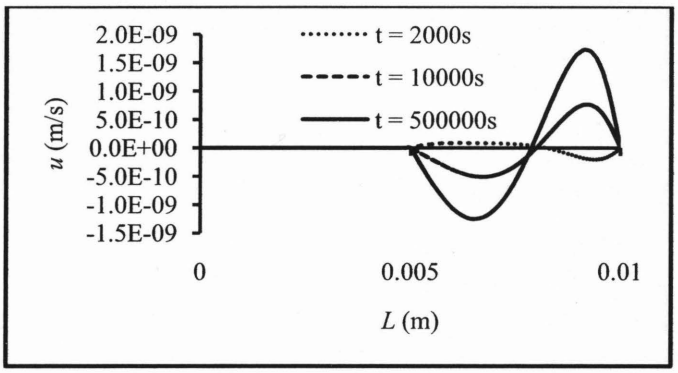

Figure 4.23 Velocity profiles at the vertical median direction

Figure 4.24 represents the isopropanol distributions in the cavity for different time steps. From this figure, it can be seen that, at the early time step (t = 2000s), the concentration of isopropanol in the liquid layer is 0.114 and in the porous layer is 0.484 (figure 4.24a). But, as the time increases, the concentrations of isopropanol both in the liquid and the porous layer are changed (figure 4.24b). When the time increases further, we can clearly see the two different effects of thermodiffusion on isopropanol distribution (figure 4.24c). Initially 90% water-10% isopropanol is set in the liquid layer. So, due to the effect of thermodiffusion (negative Soret coefficient), in the liquid layer, isopropanol molecules migrate to the hot (right) wall. And 50% water-50%

isopropanol is set in the porous layer. So, due to the effect of thermodiffusion (positive Soret coefficient), in the porous layer, isopropanol molecules migrate to the cold (left) wall.

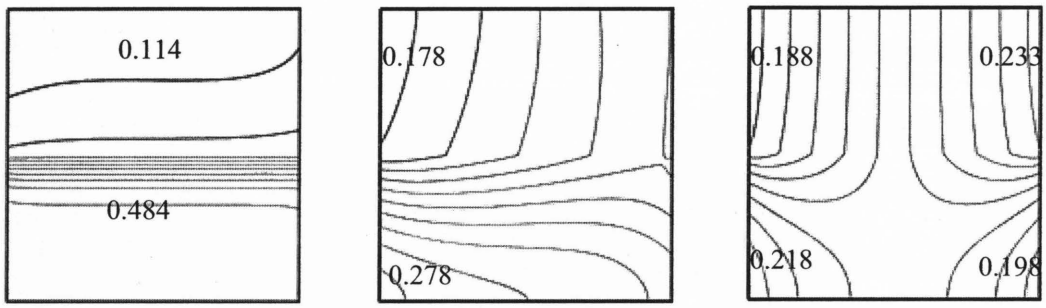

ΔC = 4.1e-2 ΔC = 1.1e-2 ΔC = 5.0e-3

(a) t = 2,000s (b) t = 100,000s (c) t = 500,000s

Figure 4.24 Isopropanol distributions

Figure 4.25 shows the isopropanol distribution for different time steps along the vertical direction of the cavity. From this figure, we can see that, initially t = 0s, the concentration of isopropanol in the porous layer is 0.50 and in the liquid layer is 0.10. But, as the time increases, the concentration of isopropanol in the porous layer gradually decreases and, in the liquid layer, gradually increases. At the time step t = 500000s, the difference in concentrations of isopropanol in the whole cavity becomes minimum.

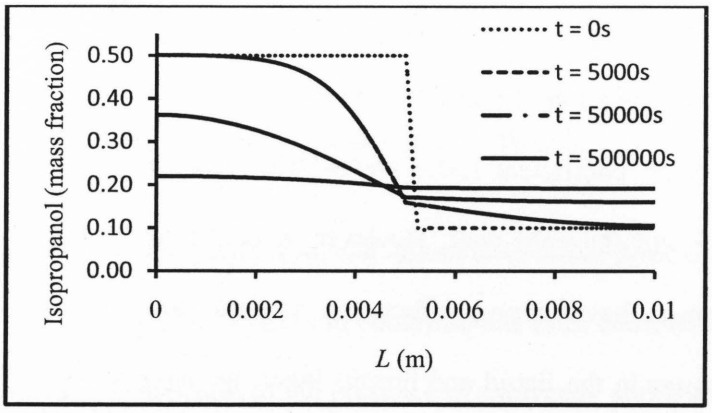

(a) Near the cold wall ($H = 0.00125$m)

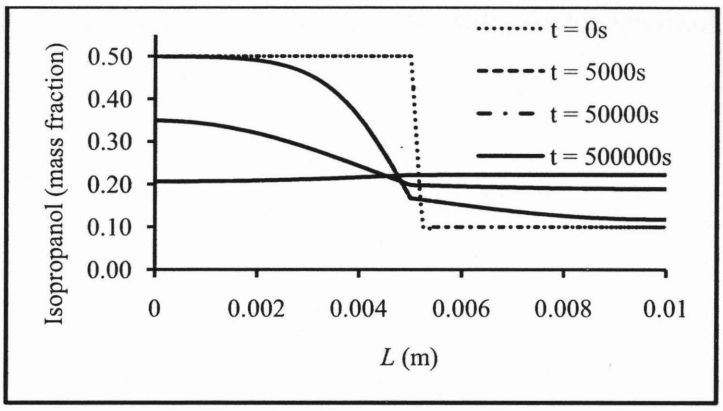

(b) Near the hot wall ($H = 0.0075$m)

Figure 4.25 Isopropanol distributions along the vertical direction

4.6 Summary

In this chapter, thermo-solutal convection and thermodiffusion convection are studied in detail. For the thermo-solutal convection, both buoyancy and Marangoni cases are studied. In the buoyancy case, the convective flows for the single and double liquid mixtures have been observed. But, due to the presence of strong buoyancy effects, the thermo-solutal effect has not been seen on convection. However, the thermo-solutal effect on convection has seen in the Marangoni case. Three different cases for the thermo-solutal convection with thermodiffusion or

the Soret effect have been studied. For the liquid with negative Soret coefficient (90% water-10% isopropanol), it has been found that isopropanol moves toward the hot wall. And, for the liquid with positive Soret coefficient (50% water-50% isopropanol), it has been found that isopropanol moves toward the cold wall. However, it has been confirmed that porosity and gravitational acceleration have strong effects on thermodiffusion. For another case with combined liquid mixtures in the liquid and porous layer, we have found that, at the early time step, multi cells appear in the liquid layer. But after crossing the diffusive characteristic time, a single cell having a clockwise rotating direction appears.

CHAPTER 5

Conclusion and Future Work

In this thesis, thermodiffusion, buoyancy and Marangoni convection have been studied in detail. A rectangular finite cavity with a lateral heating condition has been considered. Several cases are examined and they include: convection in the presence of buoyancy and thermocapillary effects, thermo-solutal convection in the presence of molecular diffusion convection and thermodiffusion.

For the buoyancy convection case, it has been found that the switching of the flow from fluid layer dominated to porous layer dominated convection depends upon the thickness ratio, aspect ratio, Prandtl number and Rayleigh number of the liquid. The convective flow occupies the entire cavity when the thickness ratio has a value of $d = 0.90$. For the Marangoni convection, it has been confirmed that the critical thickness ratio value is $d = 0.90$. Below this value, the flow is limited to the liquid layer, and above it, the flow switches to the porous layer. Also, for the Marangoni case, there is no significant change in convection due to the change of aspect ratios from 1 to 2.

For the buoyancy case with thermo-solutal convection, it has been found that the convective flow is very strong. But the Marangoni case with thermo-solutal convection is too weak as compare to the buoyancy case. For the thermo-solutal convection in the presence of thermodiffusion or the Soret effect, it has been found that isopropanol components migrate to either to hot or cold walls depending on the physical properties (Soret coefficient) of the liquid mixture. For the liquid mixture having a negative Soret coefficient, isopropanol moves towards the hot wall. However, for the liquid mixture having a positive Soret coefficient, isopropanol moves towards the cold

wall. For the case with two different water-isopropanol mixtures, a clockwise rotating direction flow was found at a time step greater than the characteristic time defined as, $\tau_D = L^2 / D_M$.

For further study, it would be interesting to analyze the thermodiffusion effect for different aspect ratios of the model, including different binary or turnery mixtures. Also, it would be interesting to observe the thermodiffusion effect in the presence of g-jitter.

APPENDIX A

Non-Dimensional Analysis of Governing Equations

The following dimensionless variables are substituted into the dimensional equations in order to render them non-dimensional:

$$U=\frac{u,}{u_o}, V=\frac{v}{v_o}, X=\frac{x}{L}, Y=\frac{y}{L}, P=\frac{p.L}{\mu.u_o}, u_o=\sqrt{g.\beta_T.\Delta T.L}, \tau=\frac{t.u_o}{L}, \theta=\frac{T-T_o}{L},$$
$$C=\frac{c-c_o}{\Delta c}, L=d_1+d_2, \mathrm{Re}=\frac{\rho_f.u_o.L}{\mu}, \mathrm{Pr}=\frac{\nu}{\alpha}, Da=\frac{\kappa}{L^2}, Ra_{LL}=\frac{g.\beta_T.\Delta T.d_1^3}{\nu\alpha},$$
$$Ra_{LC}=\frac{g.\beta_C.\Delta C.d_1^3}{\nu.\alpha}, Ra_{PL}=\frac{g.\beta_T.\Delta T.d_2.\kappa}{\nu.\alpha}, Ra_{PC}=\frac{g.\beta_C.\Delta C.d_2.\kappa}{\nu.\alpha}, Sc=\frac{\nu}{D_M} \quad \text{(A.1)}$$

A.1 Thermo-solutal Convection

A.1.1 Liquid Layer

A.1.1.1 Continuity Equation

$$\left[\frac{\partial u}{\partial x}+\frac{\partial v}{\partial y}\right]=0 \quad \text{(A.2)}$$

Substitute the non-dimensional terms

$$\left[\frac{\partial U}{\partial X}+\frac{\partial V}{\partial Y}\right]=0 \quad \text{(A.3)}$$

A.1.1.2 *X*-direction Momentum Balance equation

$$\rho_f\left[\frac{\partial u}{\partial t}+u.\frac{\partial u}{\partial x}+v.\frac{\partial u}{\partial y}\right]=-\frac{\partial p}{\partial x}+\mu\left[\frac{\partial^2 u}{\partial x^2}+\frac{\partial^2 u}{\partial y^2}\right] \quad \text{(A.4)}$$

Substitute the non-dimensional terms

$$\rho_f\left[\frac{\partial(U.u_o)}{\partial(\frac{\tau.L}{u_o})}+(U.u_o).\frac{\partial(U.u_o)}{\partial(X.L)}+(V.u_o).\frac{\partial(U.u_o)}{\partial(Y.L)}\right]=-\frac{\partial(\frac{P.\mu.u_o}{L})}{\partial(X.L)}+\mu\left[\frac{\partial}{\partial(X.L)}.\frac{\partial(U.u_o)}{\partial(X.L)}+\frac{\partial}{\partial(Y.L)}.\frac{\partial(U.u_o)}{\partial(Y.L)}\right]$$

Simplified the equation we get:

$$\text{Re}.\left[\frac{\partial U}{\partial\tau}+U.\frac{\partial U}{\partial X}+V.\frac{\partial U}{\partial Y}\right]=-\frac{\partial P}{\partial X}+\left[\frac{\partial^2 U}{\partial X^2}+\frac{\partial^2 U}{\partial Y^2}\right] \qquad \text{(A.5)}$$

Where $\text{Re}=\dfrac{\rho_f.u_o.L}{\mu}$

A.1.1.3 *Y*-direction Momentum Balance equation

$$\rho_f.\left[\frac{\partial v}{\partial t}+u.\frac{\partial v}{\partial x}+v.\frac{\partial v}{\partial y}\right]=-\frac{\partial p}{\partial y}+\mu.\left[\frac{\partial^2 v}{\partial x^2}+\frac{\partial^2 v}{\partial y^2}\right]-\rho_f.g\left[\beta_T.(T-T_o)-\beta_C.(c-c_o)\right] \qquad \text{(A.6)}$$

Substitute the non-dimensional terms and take out the common variables to get:

$$\rho_f.\frac{u_o^2}{L}.\left[\frac{\partial V}{\partial\tau}+U.\frac{\partial V}{\partial X}+V.\frac{\partial V}{\partial Y}\right]=-\frac{\mu.u_o}{L^2}.\frac{\partial P}{\partial Y}+\frac{\mu.u_o}{L^2}.\left[\frac{\partial^2 V}{\partial X^2}+\frac{\partial^2 V}{\partial Y^2}\right]-\rho_f.g.\left[\beta_T.\Delta T.\theta-\beta_C.\Delta C.C\right]$$

Where, $(T-T_o)=\Delta T.\theta$ *and* $(c-c_o)=\Delta C.C$

Multiply the above equation by the factor of $\dfrac{L^2}{\mu.u_o}$

$$\text{Re}\left[\frac{\partial V}{\partial\tau}+U.\frac{\partial V}{\partial X}+V.\frac{\partial V}{\partial Y}\right]=-\frac{\partial P}{\partial Y}+\left[\frac{\partial^2 V}{\partial X^2}+\frac{\partial^2 V}{\partial Y^2}\right]-\underbrace{\frac{L^2}{\mu.u_o}.\rho_f.g\left[\beta_T.\Delta T.\theta-\beta_C.\Delta C.C\right]}_{*}$$

Simplify the * term:

$$\frac{\rho_f.g.\beta_T.\Delta T.L^2}{\mu.u_o}.\theta-\frac{\rho_f.g.\beta_C.\Delta C.L^2}{\mu.u_o}.C$$

Substitute the thermal Rayleigh number (for the liquid layer), $Ra_{LL} = \frac{g.\beta_T.\Delta T.d_1^3}{\nu.\alpha}$ and solutal Rayleigh number (for the liquid layer), $Ra_{LC} = \frac{g.\beta_C.\Delta C.d_1^3}{\nu.\alpha}$ in the * term

So,

$$* = \frac{\rho_f.L^2.\alpha.\nu}{\mu.u_o.d_1^3}\left[Ra_{LL}.\theta - Ra_{LC}.C\right]$$

Substitute in the Prandtl number, $\Pr = \frac{\mu.(C_p)_f}{k_f}$, the thermal diffusivity of the fluid, $\alpha = \frac{k_f}{(\rho.C_p)_f}$, the Reynolds number, $\mathrm{Re} = \frac{\rho_f.u_o.L}{\mu}$ and $L = d_1 + d_2$ in the * term to obtain

$$* = \frac{1}{\Pr.\mathrm{Re}}\left[Ra_{LL}.\theta - Ra_{LC}.C\right](1+\frac{d_2}{d_1})^3$$

So the final form of the non-dimensional equation in the y-direction can be expressed as:

$$\mathrm{Re}\left[\frac{\partial V}{\partial \tau} + U.\frac{\partial V}{\partial X} + V.\frac{\partial V}{\partial Y}\right] = -\frac{\partial P}{\partial Y} + \left[\frac{\partial^2 V}{\partial X^2} + \frac{\partial^2 V}{\partial Y^2}\right] - \frac{1}{\Pr.\mathrm{Re}}.(1+\frac{d_2}{d_1})^3.\left[Ra_{LL}.\theta - Ra_{LC}.C\right] \quad \text{(A.7)}$$

A.1.1.4 Energy balance equation

$$(\rho.C_p)_f.\left[\frac{\partial T}{\partial t} + u.\frac{\partial T}{\partial x} + v.\frac{\partial T}{\partial y}\right] = k_f.\left[\frac{\partial^2 T}{\partial x^2} + \frac{\partial^2 T}{\partial y^2}\right] \quad \text{(A.8)}$$

Substitute the non-dimensional parameters to obtain:

$$(\rho.C_p)_f.\left[\frac{\Delta T.\partial\theta}{\partial(\frac{\tau.L}{u_o})} + \frac{U.u_o.\Delta T}{L}.\frac{\partial\theta}{\partial X} + \frac{V.u_o.\Delta T}{L}.\frac{\partial\theta}{\partial Y}\right] = \frac{k_f.\Delta T}{L^2}.\left[\frac{\partial^2\theta}{\partial X^2} + \frac{\partial^2\theta}{\partial Y^2}\right]$$

Extract the common variables from both left hand side and right hand side:

$$\frac{(\rho.C_p)_f.\Delta T.u_o}{L}.\left[\frac{\partial\theta}{\partial\tau}+U.\frac{\partial\theta}{\partial X}+V.\frac{\partial\theta}{\partial Y}\right]=\frac{k_f.\Delta T}{L^2}.\left[\frac{\partial^2\theta}{\partial X^2}+\frac{\partial^2\theta}{\partial Y^2}\right]$$

Multiplying above equation by the factor of $\frac{L^2}{k_f.\Delta T}$

$$\frac{\rho_f.u_o.L}{\mu}.\frac{\mu.(C_p)_f}{k_f}.\left[\frac{\partial\theta}{\partial\tau}+U.\frac{\partial\theta}{\partial X}+V.\frac{\partial\theta}{\partial Y}\right]=\left[\frac{\partial^2\theta}{\partial X^2}+\frac{\partial^2\theta}{\partial Y^2}\right]$$

Substitute the Reynolds number, $\mathrm{Re}=\frac{\rho_f.u_o.L}{\mu}$ and the Prandtl number, $\mathrm{Pr}=\frac{\mu.(C_p)_f}{k_f}$, to get the non-dimensional form of the energy balance equation

$$\mathrm{Re.Pr}.\left[\frac{\partial\theta}{\partial\tau}+U.\frac{\partial\theta}{\partial X}+V.\frac{\partial\theta}{\partial Y}\right]=\left[\frac{\partial^2\theta}{\partial X^2}+\frac{\partial^2\theta}{\partial Y^2}\right] \qquad \text{(A.9)}$$

A.1.1.5 Mass Balance equation

$$\rho_f.\left[\frac{\partial c}{\partial t}+u.\frac{\partial c}{\partial x}+v.\frac{\partial c}{\partial y}\right]=\rho_f.D_M.\left[\frac{\partial^2 c}{\partial x^2}+\frac{\partial^2 c}{\partial y^2}\right] \qquad \text{(A.10)}$$

Substitute the non-dimensional parameters to obtain:

$$\rho_f.\left[\frac{\Delta C.\partial C}{\partial(\frac{\tau.L}{u_o})}+(U.u_o).\frac{\Delta C.\partial C}{\partial(X.L)}+(V.u_o).\frac{\Delta C.\partial C}{\partial(Y.L)}\right]=\rho_f.D_M.\left[\frac{\partial}{\partial(X.L)}.\frac{\partial(\Delta C.C)}{\partial(X.L)}+\frac{\partial}{\partial(Y.L)}.\frac{\partial(\Delta C.C)}{\partial(Y.L)}\right]$$

Extract the common variables from both left hand side and right hand side:

$$\frac{\rho_f.\Delta C.u_o}{L}.\left[\frac{\partial C}{\partial\tau}+U.\frac{\partial C}{\partial X}+V.\frac{\partial C}{\partial Y}\right]=\frac{\rho_f.\Delta C.D_M}{L^2}.\left[\frac{\partial^2 C}{\partial X^2}+\frac{\partial^2 C}{\partial Y^2}\right]$$

Multiplying above equation by the factor of $\frac{L}{\rho_f.\Delta C.u_o}$

$$\left[\frac{\partial C}{\partial \tau}+U.\frac{\partial C}{\partial X}+V.\frac{\partial C}{\partial Y}\right]=\frac{D_M}{u_o.L}.\left[\frac{\partial^2 C}{\partial X^2}+\frac{\partial^2 C}{\partial Y^2}\right]$$

Now,

$$\frac{D_M}{u_o.L}=\frac{D_M}{\nu}.\frac{\nu}{u_o.L}$$

Substitute the Schmidt number, $Sc=\frac{\nu}{D_M}$ and Reynolds number, $\mathrm{Re}=\frac{u_0.L}{\nu}$, we get

$$\frac{D_M}{u_0.L}=\frac{1}{Re.Sc}$$

Finally the non-dimensional form of the mass balance equation

$$\left[\frac{\partial C}{\partial \tau}+U.\frac{\partial C}{\partial X}+V.\frac{\partial C}{\partial Y}\right]=\frac{1}{\mathrm{Re}.Sc}.\left[\frac{\partial^2 C}{\partial X^2}+\frac{\partial^2 C}{\partial Y^2}\right] \qquad \text{(A.11)}$$

A.1.2 Porous Layer

A.1.2.1 Continuity equation

The derivation of Continuity equation for porous layer is same as for liquid layer.

A.1.2.2 *X*-direction Momentum Balance equation

$$\frac{\rho_{f1}}{\phi}.\left[\frac{\partial u}{\partial t}\right]+\frac{\mu_1}{\kappa}.u=-\frac{\partial p}{\partial x}+\mu_1.\left[\frac{\partial^2 u}{\partial x^2}+\frac{\partial^2 u}{\partial y^2}\right] \qquad \text{(A.12)}$$

Substitute the non-dimensional terms

$$\frac{\rho_{f1}}{\phi}.\left[\frac{\partial(U.u_o)}{\partial(\frac{\tau.L}{u_o})}\right]+\frac{\mu_1}{\kappa}.(U.u_o)=-\frac{\partial(\frac{P.\mu_1.u_o}{L})}{\partial(X.L)}+\mu_1.\left[\frac{\partial}{\partial(X.L)}.\frac{\partial(U.u_o)}{\partial(X.L)}+\frac{\partial}{\partial(Y.L)}.\frac{\partial(U.u_o)}{\partial(Y.L)}\right]$$

Simplified the equation and substitute the Reynolds number, $\mathrm{Re}_1 = \frac{\rho_{f1}.u_o.L}{\mu_1}$ and Darcy number,

$Da = \frac{\kappa}{L^2}$ to get the non-dimensional form of the X-momentum balance equation

$$\frac{\mathrm{Re}_1}{\phi}.\left[\frac{\partial U}{\partial \tau}\right] + \frac{1}{Da}.[U] = -\frac{\partial P}{\partial X} + \left[\frac{\partial^2 U}{\partial X^2} + \frac{\partial^2 U}{\partial Y^2}\right] \tag{A.13}$$

A.1.2.3 *Y*-direction Momentum Balance equation

$$\frac{\rho_{f1}}{\phi}.\left[\frac{\partial v}{\partial t}\right] + \frac{\mu_1}{\kappa}.v = -\frac{\partial p}{\partial y} + \mu_1.\left[\frac{\partial^2 v}{\partial x^2} + \frac{\partial^2 v}{\partial y^2}\right] - \rho_{f1}.g.[\beta_{T1}.(T - T_o) - \beta_{C1}.(c - c_o)] \tag{A.14}$$

Substitute the non-dimensional terms and take out the common variables to get:

$$\frac{\rho_{f1}}{\phi}.\frac{u_o^2}{L}.\left[\frac{\partial V}{\partial \tau}\right] + \frac{\mu_1.u_o}{\kappa}.V = -\frac{\mu_1.u_o}{L^2}.\frac{\partial P}{\partial Y} + \frac{\mu_1.u_o}{L^2}.\left[\frac{\partial^2 V}{\partial X^2} + \frac{\partial^2 V}{\partial Y^2}\right] - \rho_{f1}.g.[\beta_{T1}.\Delta T.\theta - \beta_{C1}.\Delta C.C]$$

Where, $(T - T_o) = \Delta T.\theta$ *and* $(c - c_o) = \Delta C.C$

Multiply the above equation by the factor of $\frac{L^2}{\mu_1.u_o}$.

$$\frac{\mathrm{Re}_1}{\phi}.\left[\frac{\partial V}{\partial \tau}\right] + \frac{1}{Da}[V] = -\frac{\partial P}{\partial Y} + \left[\frac{\partial^2 V}{\partial X^2} + \frac{\partial^2 V}{\partial Y^2}\right] \underbrace{- \frac{L^2}{\mu_1.u_o}.\rho_{f1}.g.[\beta_{T1}.\Delta T.\theta - \beta_{C1}.\Delta C.C]}_{**}$$

Simplify the ** term:

$$\frac{\rho_{f1}.g.\beta_{T1}.\Delta T.L^2}{\mu_1.u_o}.\theta - \frac{\rho_{f1}.g.\beta_{C1}.\Delta C.L^2}{\mu_1.u_o}.C$$

Substitute the thermal Rayleigh number (for the porous layer), $Ra_{PL} = \frac{g.\beta_{T1}.\Delta T.d_2.\kappa}{\nu_1.\alpha_1}$ and solutal

Rayleigh number (for the porous layer), $Ra_{PC} = \frac{g.\beta_{C1}.\Delta C.d_2.\kappa}{\nu_1.\alpha_1}$,the Prandtl number

$\mathrm{Pr}_1 = \frac{\mu_1.(C_p)_{f1}}{k_{f1}}$, the thermal diffusivity of the fluid $\alpha_1 = \frac{k_{f1}}{(\rho.C_p)_{f1}}$, the Reynolds number,

$\mathrm{Re}_1 = \frac{\rho_{f1}.u_o.L}{\mu_1}$, the Darcy number $Da = \frac{\kappa}{L^2}$ and $L = d_1 + d_2$ we get,

$$** = \frac{1}{\mathrm{Pr}_1.\mathrm{Re}_1.Da}.[Ra_{PL}.\theta - Ra_{PC}.C].(1+\frac{d_2}{d_1})^3$$

So the final form of the non-dimensional equation in the y-direction can be expressed as:

$$\frac{\mathrm{Re}_1}{\phi}.\left[\frac{\partial V}{\partial \tau}\right] + \frac{1}{Da}.[V] = -\frac{\partial P}{\partial Y} + \left[\frac{\partial^2 V}{\partial X^2} + \frac{\partial^2 V}{\partial Y^2}\right] - \left[\frac{1}{\mathrm{Pr}_1.\mathrm{Re}_1.Da}\right].(1+\frac{d_2}{d_1})^3.[Ra_{PL}.\theta - Ra_{PC}.C] \quad \text{(A.15)}$$

A.1.2.4 Energy equation for porous layer

$$(\rho.C_p)_{f1}.\left[\frac{\partial T}{\partial t} + u.\frac{\partial T}{\partial x} + v.\frac{\partial T}{\partial y}\right] = k_e.\left[\frac{\partial^2 T}{\partial x^2} + \frac{\partial^2 T}{\partial y^2}\right] \quad \text{(A.16)}$$

Substitute the non-dimensional parameters to obtain:

$$(\rho.C_p)_{f1}.\left[\frac{\Delta T.\partial\theta}{\partial(\frac{\tau.L}{u_o})} + \frac{U.u_o.\Delta T}{L}.\frac{\partial\theta}{\partial X} + \frac{V.u_o.\Delta T}{L}.\frac{\partial\theta}{\partial Y}\right] = \frac{k_e.\Delta T}{L^2}.\left[\frac{\partial^2\theta}{\partial X^2} + \frac{\partial^2\theta}{\partial Y^2}\right]$$

Extract the common variables from both left hand side and right hand side:

$$\frac{(\rho.C_p)_{f1}.\Delta T.u_o}{L}.\left[\frac{\partial\theta}{\partial\tau} + U.\frac{\partial\theta}{\partial X} + V.\frac{\partial\theta}{\partial Y}\right] = \frac{k_e.\Delta T}{L^2}.\left[\frac{\partial^2\theta}{\partial X^2} + \frac{\partial^2\theta}{\partial Y^2}\right]$$

Multiplying above equation by the factor of $\frac{L^2}{k_{f1}.\Delta T}$

$$\frac{\rho_{f1}.u_o.L}{\mu}.\frac{\mu.(C_p)_{f1}}{k_{f1}}.\left[\frac{\partial\theta}{\partial\tau}+U.\frac{\partial\theta}{\partial X}+V.\frac{\partial\theta}{\partial Y}\right]=\frac{k_e}{k_{f1}}\left[\frac{\partial^2\theta}{\partial X^2}+\frac{\partial^2\theta}{\partial Y^2}\right]$$

Substitute the Reynolds number $\mathrm{Re}_1=\frac{\rho_{f1}.u_o.L}{\mu_1}$ and the Prandtl number $\mathrm{Pr}_1=\frac{\mu_1.(C_p)_{f1}}{k_{f1}}$, to get the non-dimensional form of the energy balance equation

$$\mathrm{Re}_1.\mathrm{Pr}_1.\left[\frac{\partial\theta}{\partial\tau}+U.\frac{\partial\theta}{\partial X}+V.\frac{\partial\theta}{\partial Y}\right]=G\left[\frac{\partial^2\theta}{\partial X^2}+\frac{\partial^2\theta}{\partial Y^2}\right] \quad \text{(A.17)}$$

Where, $G=\frac{k_e}{k_{f1}}=\frac{\phi.k_{f1}+(1-\phi).k_s}{k_{f1}}=\phi+(1-\phi).\frac{k_s}{k_{f1}}$ (A.18)

Also k_e is the effective thermal conductivity, k_{f1} is conductivity of the fluid, k_s is the conductivity of the solid, and G is the non-dimensional overall thermal conductivity.

A.1.2.5 Mass Balance Equation

The mass balance equation for the porous layer is the same as the mass balance equation for the liquid layer.

A.2 Thermodiffusion Convection

A.2.1 Liquid Layer

The Continuity, Momentum balance and the Energy balance equations for thermodiffusion case (in the liquid layer) are the same as for the molecular diffusion case (equations A.2 to A.9). But the Mass balance equation for the thermodiffusion case is different from molecular diffusion.

A.2.1.1 Mass Balance equation for the liquid layer

$$\rho_f.\left[\frac{\partial c}{\partial t}+u.\frac{\partial c}{\partial x}+v.\frac{\partial c}{\partial y}\right]=\rho_f.D_M.\left[\frac{\partial^2 c}{\partial x^2}+\frac{\partial^2 c}{\partial y^2}\right]+\rho_f.D_T.\left[\frac{\partial^2 T}{\partial x^2}+\frac{\partial^2 T}{\partial y^2}\right] \quad \text{(A.19)}$$

Substitute the non-dimensional parameters to obtain:

$$\rho_f.\left[\frac{\Delta C.\partial C}{\partial(\frac{\tau.L}{u_o})}+U.u_o.\frac{\Delta C.\partial C}{\partial(X.L)}+V.u_o.\frac{\Delta C.\partial C}{\partial(Y.L)}\right]=\rho_f.D_M.\left[\frac{\partial}{\partial(X.L)}.\frac{\partial(\Delta C.C)}{\partial(X.L)}+\frac{\partial}{\partial(Y.L)}.\frac{\partial(\Delta C.C)}{\partial(Y.L)}\right]$$

$$+\rho_f.D_T.\left[\frac{\partial}{\partial(X.L)}.\frac{\partial(\Delta T.\theta)}{\partial(X.L)}+\frac{\partial}{\partial(Y.L)}.\frac{\partial(\Delta T.\theta)}{\partial(Y.L)}\right]$$

Extract the common variables from both left hand side and right hand side:

$$\frac{\rho_f.\Delta C.u_o}{L}.\left[\frac{\partial C}{\partial \tau}+U.\frac{\partial C}{\partial X}+V.\frac{\partial C}{\partial Y}\right]=\frac{\rho_f.\Delta C.D_M}{L^2}.\left[\frac{\partial^2 C}{\partial X^2}+\frac{\partial^2 C}{\partial Y^2}\right]+\frac{\rho_f.\Delta T.D_T}{L^2}.\left[\frac{\partial^2 \theta}{\partial X^2}+\frac{\partial^2 \theta}{\partial Y^2}\right]$$

Multiplying above equation by the factor of $\frac{L}{\rho_f.\Delta C.u_o}$

$$\left[\frac{\partial C}{\partial \tau}+U.\frac{\partial C}{\partial X}+V.\frac{\partial C}{\partial Y}\right]=\frac{D_M}{u_o.L}.\left[\frac{\partial^2 C}{\partial X^2}+\frac{\partial^2 C}{\partial Y^2}\right]+\frac{D_T.\Delta T}{u_o.L.\Delta C}\left[\frac{\partial^2 \theta}{\partial X^2}+\frac{\partial^2 \theta}{\partial Y^2}\right]$$

Now,

$$\frac{D_M}{u_o.L}=\frac{D_M}{\nu}.\frac{\nu}{u_o.L}$$

$$=\frac{\nu}{Sc.u_o.L}$$

Where, Schmidt number, $Sc=\frac{\mu}{\rho_f.D_M}$

We have, characteristic velocity, $u_o=\sqrt{g.\beta_T.\Delta T.L}$

So

$$\frac{\nu}{u_o.L} = \sqrt{\frac{\nu^2}{g.\beta_T.\Delta T.L^3}}$$

$$= \sqrt{\frac{\nu.\alpha}{g.\beta_T.\Delta T.d_1^3}.\frac{\nu.d_1^3}{\alpha.L^3}}$$

$$= \sqrt{\frac{\nu.d_1^3}{Ra_{LL}.\alpha.L^3}}$$

$$= \sqrt{\frac{\Pr}{Ra_{LL}}}.\left[\frac{d_1}{d_1+d_2}\right]^{\frac{3}{2}}$$

$$= \sqrt{\frac{\Pr}{Ra_{LL}}}.\left[1+\frac{d_2}{d_1}\right]^{-\frac{3}{2}}$$

And,

$$\frac{D_T.\Delta T}{u_o.L.\Delta C} = \frac{D_M.S_T.\Delta T}{u_o.L.\Delta C}$$

$$= \alpha_T.\frac{D_M}{u_o.L.\Delta C}$$

$$= \frac{D_M}{\nu}.\frac{\nu.\alpha_T}{u_o.L.1}$$

$$= \frac{\alpha_T}{Sc}.\frac{\nu}{u_0.L}$$

$$= \frac{\alpha_T}{Sc}.\sqrt{\frac{\Pr}{Ra_{LL}}}.\left[1+\frac{d_2}{d_1}\right]^{-\frac{3}{2}}$$

Where the Soret coefficient, $S_T = \frac{D_T}{D_M}$, $\alpha_T = \Delta T.S_T$, solutal difference, ΔC = 1, Prandtl number,

$\Pr = \frac{\mu.C_p}{\kappa_f}$ and liquid Rayleigh number (in liquid layer), $Ra_{LL} = \frac{g.\beta_T.\Delta T.d_1^3}{\nu.\alpha}$

Finally the non-dimensional form of the mass balance equation

$$\left[\frac{\partial C}{\partial \tau}+U.\frac{\partial C}{\partial X}+V.\frac{\partial C}{\partial Y}\right] = \frac{1}{Sc}.\sqrt{\frac{\Pr}{Ra_{LL}}}.\left[1+\frac{d_2}{d_1}\right]^{-\frac{3}{2}}\left\{\left[\frac{\partial^2 C}{\partial X^2}+\frac{\partial^2 C}{\partial Y^2}\right]+\alpha_T.\left[\frac{\partial^2 \theta}{\partial X^2}+\frac{\partial^2 \theta}{\partial Y^2}\right]\right\} \quad \text{(A.20)}$$

A.2.2 Porous Layer

For the porous layer we have two different situations: (1) the compositions of the liquid both in the liquid layer and in the porous layer are the same, (2) the compositions of the liquid in the liquid layer is different from the porous layer.

A.2.2.1 For the case when same compositions present both in the liquid and in the porous layer

A.2.2.1.1 Continuity equation

The derivation of Continuity equation for porous layer is same as for liquid layer.

A.2.2.1.2 *X*-direction Momentum Balance equation

$$\frac{\rho_f}{\phi}.\left[\frac{\partial u}{\partial t}\right]+\frac{\mu}{\kappa}.u=-\frac{\partial p}{\partial x}+\mu.\left[\frac{\partial^2 u}{\partial x^2}+\frac{\partial^2 u}{\partial y^2}\right] \qquad \text{(A.22)}$$

Substitute the non-dimensional terms

$$\frac{\rho_f}{\phi}.\left[\frac{\partial(U.u_o)}{\partial(\frac{\tau.L}{u_o})}\right]+\frac{\mu}{\kappa}.(U.u_o)=-\frac{\partial(\frac{P.\mu.u_o}{L})}{\partial(X.L)}+\mu.\left[\frac{\partial}{\partial(X.L)}.\frac{\partial(U.u_o)}{\partial(X.L)}+\frac{\partial}{\partial(Y.L)}.\frac{\partial(U.u_o)}{\partial(Y.L)}\right]$$

Simplified the equation by taking out the common variables on both the left hand side and right hand side:

$$\frac{\rho_f}{\phi}.\frac{u_o^2}{L}\left[\frac{\partial U}{\partial \tau}\right]+\frac{\mu.u_o}{\kappa}.U=-\frac{\mu.u_o}{L^2}.\frac{\partial P}{\partial X}+\frac{\mu.u_o}{L^2}.\left[\frac{\partial^2 U}{\partial X^2}+\frac{\partial^2 U}{\partial Y^2}\right]$$

Multiplying above equations by a factor of $\frac{L^2}{\mu.u_o}$ to further simplify the equation:

$$\frac{\rho_f.u_o.L}{\phi.\mu}.\left[\frac{\partial U}{\partial \tau}\right]+\frac{L^2}{\kappa}.U=-\frac{\partial P}{\partial X}+\left[\frac{\partial^2 U}{\partial X^2}+\frac{\partial^2 U}{\partial Y^2}\right]$$

Substitute the Reynolds number, $\mathrm{Re}=\frac{\rho_f.u_o.L}{\mu}$ and Darcy number, $Da=\frac{\kappa}{L^2}$ to get the non-dimensional form of the X-momentum balance equation

$$\mathrm{Re}\frac{\mathrm{Re}}{\phi}.\left[\frac{\partial U}{\partial \tau}\right]+\frac{1}{Da}.[U]=-\frac{\partial P}{\partial X}+\left[\frac{\partial^2 U}{\partial X^2}+\frac{\partial^2 U}{\partial Y^2}\right] \qquad \text{(A.23)}$$

A.2.2.1.3 *Y*-direction Momentum Balance equation

$$\frac{\rho_f}{\phi}.\left[\frac{\partial v}{\partial t}\right]+\frac{\mu}{\kappa}.v=-\frac{\partial p}{\partial y}+\mu.\left[\frac{\partial^2 v}{\partial x^2}+\frac{\partial^2 v}{\partial y^2}\right]-\rho_f.g.[\beta_T.(T-T_o)-\beta_C.(c-c_o)] \qquad \text{(A.24)}$$

Substitute the non-dimensional terms and take out the common variables to get:

$$\frac{\rho_f}{\phi}.\frac{u_o^2}{L}.\left[\frac{\partial V}{\partial \tau}\right]+\frac{\mu.u_o}{\kappa}.V=-\frac{\mu.u_o}{L^2}.\frac{\partial P}{\partial Y}+\frac{\mu.u_o}{L^2}.\left[\frac{\partial^2 V}{\partial X^2}+\frac{\partial^2 V}{\partial Y^2}\right]-\rho_f.g.[\beta_T.\Delta T.\theta-\beta_C.\Delta C.C]$$

Where, $(T-T_o)=\Delta T.\theta$ *and* $(c-c_o)=\Delta C.C$

Multiply the above equation by the factor of $\frac{L^2}{\mu.u_o}$.

$$\frac{\mathrm{Re}}{\phi}.\left[\frac{\partial V}{\partial \tau}\right]+\frac{1}{Da}[V]=-\frac{\partial P}{\partial Y}+\left[\frac{\partial^2 V}{\partial X^2}+\frac{\partial^2 V}{\partial Y^2}\right]-\underbrace{\frac{L^2}{\mu.u_o}.\rho_f.g.[\beta_T.\Delta T.\theta-\beta_C.\Delta C.C]}_{***}$$

Simplify the *** term:

$$\frac{\rho_f.g.\beta_T.\Delta T.L^2}{\mu.u_o}.\theta-\frac{\rho_f.g.\beta_C.\Delta C.L^2}{\mu.u_o}.C$$

Substitute the thermal Rayleigh number (for the porous layer), $Ra_{PL} = \frac{g.\beta_T.\Delta T.d_2.\kappa}{\nu.\alpha}$ and solutal Rayleigh number (for the porous layer), $Ra_{PC} = \frac{g.\beta_C.\Delta C.d_2.\kappa}{\nu.\alpha}$ in the *** term, we get

$$*** = \frac{\alpha.L^2.}{u_o.\kappa.d_2}.[Ra_{PL}.\theta - Ra_{PC}.C]$$

Substitute in the Prandtl number $\Pr = \frac{\mu.(C_p)_f}{k_f}$, the thermal diffusivity of the fluid $\alpha = \frac{k_f}{(\rho.C_p)_f}$, the Reynolds number, $\mathrm{Re} = \frac{\rho_f.u_o.L}{\mu}$ and the Darcy number $Da = \frac{\kappa}{L^2}$ we get

$$\frac{1}{\Pr.\mathrm{Re}.Da}.\frac{L^3}{d_1^3}[Ra_{PL}.\theta - Ra_{PC}.C]$$

Noting that $L = d_1 + d_2$, the equation becomes

$$\frac{1}{\Pr.\mathrm{Re}.Da}.[Ra_{PL}.\theta - Ra_{PC}.C](1+\frac{d_2}{d_1})^3$$

So the final form of the non-dimensional equation in the y-direction can be expressed as:

$$\frac{\mathrm{Re}}{\phi}.\left[\frac{\partial V}{\partial \tau}\right] + \frac{1}{Da}.[V] = -\frac{\partial P}{\partial Y} + \left[\frac{\partial^2 V}{\partial X^2} + \frac{\partial^2 V}{\partial Y^2}\right] - \left[\frac{1}{\Pr.\mathrm{Re}.Da}\right].(1+\frac{d_2}{d_1})^3.[Ra_{PL}.\theta - Ra_{PC}.C] \quad \text{(A.25)}$$

A.2.2.1.4 Energy equation for porous layer

$$(\rho.C_p)_f.\left[\frac{\partial T}{\partial t} + u.\frac{\partial T}{\partial x} + v.\frac{\partial T}{\partial y}\right] = k_e.\left[\frac{\partial^2 T}{\partial x^2} + \frac{\partial^2 T}{\partial y^2}\right] \quad \text{(A.26)}$$

Substitute the non-dimensional parameters to obtain:

$$(\rho.C_p)_f.\left[\frac{\Delta T.\partial\theta}{\partial(\frac{\tau.L}{u_o})}+\frac{U.u_o.\Delta T}{L}.\frac{\partial\theta}{\partial X}+\frac{V.u_o.\Delta T}{L}.\frac{\partial\theta}{\partial Y}\right]=\frac{k_e.\Delta T}{L^2}.\left[\frac{\partial^2\theta}{\partial X^2}+\frac{\partial^2\theta}{\partial Y^2}\right]$$

Extract the common variables from both left hand side and right hand side:

$$\frac{(\rho.C_p)_f.\Delta T.u_o}{L}.\left[\frac{\partial\theta}{\partial\tau}+U.\frac{\partial\theta}{\partial X}+V.\frac{\partial\theta}{\partial Y}\right]=\frac{k_e.\Delta T}{L^2}.\left[\frac{\partial^2\theta}{\partial X^2}+\frac{\partial^2\theta}{\partial Y^2}\right]$$

Multiplying above equation by the factor of $\frac{L^2}{k_f.\Delta T}$

$$\frac{\rho_f.u_o.L}{\mu}.\frac{\mu.(C_p)_f}{k_f}.\left[\frac{\partial\theta}{\partial\tau}+U.\frac{\partial\theta}{\partial X}+V.\frac{\partial\theta}{\partial Y}\right]=\frac{k_e}{k_f}\left[\frac{\partial^2\theta}{\partial X^2}+\frac{\partial^2\theta}{\partial Y^2}\right]$$

Substitute the Reynolds number $\mathrm{Re}=\frac{\rho_f.u_o.L}{\mu}$ and the Prandtl number $\mathrm{Pr}=\frac{\mu.(C_p)_f}{k_f}$, to get the non-dimensional form of the energy balance equation

$$\mathrm{Re.Pr}.\left[\frac{\partial\theta}{\partial\tau}+U.\frac{\partial\theta}{\partial X}+V.\frac{\partial\theta}{\partial Y}\right]=G\left[\frac{\partial^2\theta}{\partial X^2}+\frac{\partial^2\theta}{\partial Y^2}\right] \qquad \text{(A.27)}$$

Where, $G=\frac{k_e}{k_f}=\frac{\phi.k_f+(1-\phi).k_s}{k_f}=\phi+(1-\phi).\frac{k_s}{k_f}$ (A.28)

Also k_e is the effective thermal conductivity, k_f is the conductivity of the fluid, k_s is the conductivity of the solid, and G is the non-dimensional overall thermal conductivity.

A.2.2.1.5 Mass balance equation for porous layer

The mass balance equation for the porous layer (when same compositions present both in the liquid and in the porous layer) is the same as for the liquid layer (equation A.20).

A.2.2.2 For the case when different compositions present in the liquid and in the porous layer

When different compositions present in the liquid layer and in the porous layer, the Continuity equation, the Momentum balance equations and the Energy balance equation are the same as the case of molecular diffusion (equations A.12). But the Mass balance equation for the thermodiffusion case is different from the molecular diffusion case.

A.2.2.2.1 Mass Balance equation for the liquid layer

$$\rho_{f1}.\left[\frac{\partial c}{\partial t}+u.\frac{\partial c}{\partial x}+v.\frac{\partial c}{\partial y}\right]=\rho_{f1}.D_{M1}.\left[\frac{\partial^2 c}{\partial x^2}+\frac{\partial^2 c}{\partial y^2}\right]+\rho_f.D_{T1}.\left[\frac{\partial^2 T}{\partial x^2}+\frac{\partial^2 T}{\partial y^2}\right] \qquad (A.29)$$

Substitute the non-dimensional parameters to obtain:

$$\rho_{f1}.\left[\frac{\Delta C.\partial C}{\partial(\frac{\tau.L}{u_o})}+U.u_o.\frac{\Delta C.\partial C}{\partial(X.L)}+V.u_o.\frac{\Delta C.\partial C}{\partial(Y.L)}\right]=\rho_{f1}.D_{M1}.\left[\frac{\partial}{\partial(X.L)}.\frac{\partial(\Delta C.C)}{\partial(X.L)}+\frac{\partial}{\partial(Y.L)}.\frac{\partial(\Delta C.C)}{\partial(Y.L)}\right]$$

$$+\rho_f.D_{T1}.\left[\frac{\partial}{\partial(X.L)}.\frac{\partial(\Delta T.\theta)}{\partial(X.L)}+\frac{\partial}{\partial(Y.L)}.\frac{\partial(\Delta T.\theta)}{\partial(Y.L)}\right]$$

Extract the common variables from both left hand side and right hand side:

$$\frac{\rho_{f1}.\Delta C.u_o}{L}.\left[\frac{\partial C}{\partial \tau}+U.\frac{\partial C}{\partial X}+V.\frac{\partial C}{\partial Y}\right]=\frac{\rho_{f1}.\Delta C.D_{M1}}{L^2}.\left[\frac{\partial^2 C}{\partial X^2}+\frac{\partial^2 C}{\partial Y^2}\right]+\frac{\rho_{f1}.\Delta T.D_{T1}}{L^2}.\left[\frac{\partial^2 \theta}{\partial X^2}+\frac{\partial^2 \theta}{\partial Y^2}\right]$$

Multiplying above equation by the factor of $\frac{L}{\rho_{f1}.\Delta C.u_o}$

$$\left[\frac{\partial C}{\partial \tau}+U.\frac{\partial C}{\partial X}+V.\frac{\partial C}{\partial Y}\right]=\frac{D_{M1}}{u_o.L}.\left[\frac{\partial^2 C}{\partial X^2}+\frac{\partial^2 C}{\partial Y^2}\right]+\frac{D_{T1}.\Delta T}{u_o.L.\Delta C}.\left[\frac{\partial^2 \theta}{\partial X^2}+\frac{\partial^2 \theta}{\partial Y^2}\right]$$

Now,

$$\frac{D_{M1}}{u_o.L} = \frac{D_{M1}}{\nu_1}.\frac{\nu_1}{u_o.L}$$
$$= \frac{1}{Sc_1.\mathrm{Re}_1}$$

Where, Schmidt number, $Sc_1 = \frac{\nu_1}{D_{M1}}$ and $Re_1 = \frac{u_0.L}{\nu_1}$

And,

$$\frac{D_{T1}.\Delta T}{u_o.L.\Delta C} = \frac{D_{M1}.S_{T1}.\Delta T}{u_o.L.\Delta C}$$
$$= \alpha_{T1}.\frac{D_{M1}}{u_o.L.\Delta C}$$
$$= \frac{D_{M1}}{\nu_1}.\frac{\nu_1.\alpha_{T1}}{u_o.L.1}$$
$$= \frac{\alpha_{T1}}{Sc_1}.\frac{\nu_1}{u_0.L}$$
$$= \frac{\alpha_{T1}}{Sc_1.\mathrm{Re}_1}$$

Where the Soret coefficient, $S_{T1} = \frac{D_{T1}}{D_{M1}}$, $\alpha_{T1} = \Delta T.S_{T1}$, solutal difference, $\Delta C = 1$.

Finally the non-dimensional form of the mass balance equation

$$\left[\frac{\partial C}{\partial \tau} + U.\frac{\partial C}{\partial X} + V.\frac{\partial C}{\partial Y}\right] = \frac{1}{Sc_1.\mathrm{Re}_1}.\left\{\left[\frac{\partial^2 C}{\partial X^2} + \frac{\partial^2 C}{\partial Y^2}\right] + \alpha_{T1}.\left[\frac{\partial^2 \theta}{\partial X^2} + \frac{\partial^2 \theta}{\partial Y^2}\right]\right\} \quad \text{(A.30)}$$

APPENDIX B

Input Files

B.1 Buoyancy Convection

```
Title

Buoyancy Convection in Fluid/Porous Laterally Heated Cavity

/lateral heating Bouncy case

fimesh(2-d, imax=5, jmax=5)

expi

/1  2  3  4  5

/1  0 15  0 29

1  0  121  0  241

expj

/1  2  3  4  5

/1  0 15  0 29

1  0  41  0  81

/

/physical dimension of the problem

/the aspect ratio is varied here from 1 to 6 for different cases

$ar=1

$ar1=$ar/2

/the thickness of the liquid and porous layer is varied here

$d1=0.5
```

```
$d2=0.5
$1=$d1+$d2
/
point
/n i j k x  y z
 1 5 1 1 $ar 0 0
 2 5 3 1 $ar $d2 0
 3 5 5 1 $ar $1 0
 4 3 1 1 $ar1 0 0
 5 3 3 1 $ar1 $d2 0
 6 3 5 1 $ar1 $1 0
 7 1 1 1 0. 0. 0
 8 1 3 1 0. $d2 0
 9 1 5 1 0. $1 0
line
/1st Plane
2 1
5 4
8 7
2 3 5.5 4
5 6 5.5 4
8 9 5.5 4
4 1 5.5 4
```

5 2 5.5 4

6 3 5.5 4

4 7 5.5 4

5 8 5.5 4

6 9 5.5 4

surface

1 8

2 9

elements(continuum,quad,nodes=9,entity="porous")

7 2

elements(continuum,quad,nodes=9,entity="fluid")

8 3

elements(boundary,edge,nodes=3,entity="interface")

8 2

elements(boundary,edge,nodes=3,entity="freec")

3 9

bcnode(coordinate)

3 3

9 9

/define a temperature of 1 for the right vertical wall and 0 for left wall

bcnode(temperature,constant)

1 3 1

7 9 0

bcnode(uy,constant)

3 9 0

1 7 0

bcnode(surface,constant)

3 9 0

bcnode(ux, constant)

1 2 0

7 8 0

bcnode(velocity,constant)

2 3 0

3 9 0

8 9 0

/

/

/Physical parameters

/

/the physical parameters can be varied depending on the case studied

$da=1e-5

$por=0.39

$biot=1

$pr=10.85

$ra1=8.29e4

$tr1=(1+($d2/$d1))^3

```
$re=($tr1*$ra1/$pr)^0.5
/
end
fiprep
problem(2-D, buoyancy, fixed, nonlinear)
pressure(mixed=1.0e-8, disc)
execution(newjob)
solution(segr=2000,velconv=0.001,normal=40,ncgc=1e-6,scgc=1e-6)
option(stress-divergence)
relax
0.12  0.12  0.12  0.0  0.01  0.6
density(set=1, constant=$re)
specificheat(set=1, constant=$pr)
viscosity(set=1, constant=1)
conductivity(set=1, constant=1)
conductivity(set=2, constant=1.43)
permeability(acoef, constant=1, x=$da, y=$da, porosity=$por)
gravity(magnitude=1)
htransfer(constant=$biot, temperature, reftemp=0)
renumber(profile)
entity(name="porous", porous, maperm=1, mscond=2)
entity(name="fluid", fluid)
entity(name="freec", convection, attach="fluid")
```

```
entity(name="interface", plot, attach="porous")

end

create(FISOLV)
```

B.2 Thermo-solutal convection

```
Title

Buoyancy Convection with mass diffusion in Fluid/Porous Laterally Heated Cavity

/lateral heating Diffusion case

fimesh(2-d, imax=5, jmax=5)

expi

/1  2  3  4  5

/1  0 15  0  29

1  0  121  0  241

expj

/1  2  3  4  5

/1  0 15  0 57

1  0  41  0  81

/

/physical dimension of the problem

/the aspect ratio is varied here from 1 to 6 for different cases

$ar=1

$ar1=$ar/2

/the thickness of the liquid and porous layer is varied here
```

```
$d1=0.5

$d2=0.5

$1=$d1+$d2

/

point

/n i j k x  y z

 1 5 1 1 $ar 0 0

 2 5 3 1 $ar $d2 0

 3 5 5 1 $ar $1 0

 4 3 1 1 $ar1 0 0

 5 3 3 1 $ar1 $d2 0

 6 3 5 1 $ar1 $1 0

 7 1 1 1 0. 0. 0

 8 1 3 1 0. $d2 0

 9 1 5 1 0. $1 0

line

/1st Plane

2 1

5 4

8 7

2 3 5.5 4

5 6 5.5 4

8 9 5.5 4
```

4 1 5.5 4

5 2 5.5 4

6 3 5.5 4

4 7 5.5 4

5 8 5.5 4

6 9 5.5 4

surface

1 8

2 9

elements(boundary,edge,nodes=3,entity="free")

3 9

elements(continuum,quad,nodes=9,entity="porous")

7 2

elements(continuum,quad,nodes=9,entity="fluid")

8 3

elements(boundary,edge,nodes=3,entity="interface")

8 2

elements(boundary,edge,nodes=3,entity="freec")

3 9

bcnode(coordinate)

3 3

9 9

/define a temperature of 1 for the right vertical wall and 0 for left wall

bcnode(temperature,constant)

1 3 1

7 9 0

bcnode(uy,constant)

3 9 0

1 7 0

bcnode(surface,constant)

3 9 0

bcnode(ux, constant)

1 2 0

7 8 0

bcnode(velocity,constant)

2 3 0

8 9 0

3 9 0

/

/

/Physical parameters

/

/the physical parameters can be varied depending on the case studied

/Common physical parameters

$da=1e-5

$por=0.39

```
$biot=1.0
$tr1=(1+($d2/$d1))^3
/
/Physical parameters for 10% isopropanol-90% water
/
$pr1=10.85
$ra1=1.036e4
$ra21=9.36e5
$sc1=1620.69
$re1=($tr1*$ra1/$pr1)^0.5
$betac1=$ra21/$ra1
$diff1=1.0/(($re1)*($sc1))
/
/Physical parameters for 50% isopropanol-50% water
/
$pr4=49.165
$ra4=1.33e4
$ra24=8.62e5
$sc4=23216.667
$re4=($tr1*$ra4/$pr4)^0.5
$betac4=$ra24/$ra4
$diff4=1.0/(($re4)*($sc4))
/
```

```
end
fiprep
problem(nonlinear, 2-D, buoyancy,buoyancy=1,fixed,transient)
timeint(back,dt=0.000001,nofix=5,nsteps=1000,tend=800,species=1)
pressure(mixed=1.0e-8, disc)
execution(newjob)
solution(segr=2000,velconv=0.000001,normal=40)
option(stress-divergence)
relax
0.12  0.12  0.12  0.0  0.01  0.6
density(set=1,constant=$re1,TYP2,temperature,species=1)
density(set=4,constant=$re4,TYP2,temperature,species=1)
specificheat(set=1,constant=$pr1)
specificheat(set=4,constant=$pr4)
viscosity(set=1,constant=1)
viscosity(set=4,constant=1)
conductivity(set=1, constant=1)
conductivity(set=3, constant=1.43)
conductivity(set=4,constant=1)
permeability(acoef, constant=1, x=$da, y=$da, porosity=$por)
volumexpansion(set=1,constant=1,temperature)
volumexpansion(set=2,constant=$betac1,species=1)
volumexpansion(set=4,constant=1,temperature)
```

```
volumexpansion(set=5,constant=$betac4,species=1)
gravity(magnitude=1)
diffusivity(set=2,constant=$diff1,species=1)
diffusivity(set=5,constant=$diff4,species=1)
htransfer(constant=$biot,temperature,reftemp=0)
renumber(profile)
icnode(species=1,constant=0.1,entity="fluid")
icnode(species=1,constant=0.5,entity="porous")
entity(name="porous",porous,property="4",mdiff=5,species=1,mexp=5,maperm=1,mscond=3)
entity(name="fluid", fluid,property="1", mdiff=2,species=1,mexp=2)
entity(name="free", surface)
entity(name="freec", convection, attach="fluid")
entity(name="interface", plot, attach="porous")
end
create(FISOLV)
```

APPENDIX C

Physical Properties

Table 1 The physical properties of water-isopropanol for two different compositions

Physical Properties	Symbol	90% water-10% isopropanol (mass fraction)	50% water-50% isopropanol (mass fraction)
Viscosity[m^2/s]	v	1.41E-06	4.18E-06
Thermal diffusivity [m^2/s]	a or α_T	1.30E-07	8.50E-08
Diffusion coefficient [m^2/s]	D_M or α_C	8.70E-10	1.80E-10
Thermodiffusion coefficient [$m^2/s.K$]	D_T	-9.222E-12	9.81E-13
Density [kg/m^3]	ρ	984	905
Soret coefficient [1/K]	S_T	-1.06E-02	5.45E-03
Thermal expansion [1/K]	β_T	3.10E-04	7.70E-04
Solutal expansion	β_C	0.14	-0.25
Length [m]	L	0.01	0.01
Concentration of water	Co	0.90	0.50
Pr	v/a	10.846	49.165
A	Gr/g	1559.278	440.906
Sc	v/D	1620.690	23216.667
τ_{visc} [s]	L^2/v	70.922	23.929
τ_{th} [s]	L^2/α	769.23	1176.47
τ_D [s]	L^2/D_M	11.49e4	55.56e4
Thermal conductivity[W/m.K]	k	0.522	0.2866

REFERENCES

[1] M.Z. Saghir, P. Mahendran and M. Hennenberg, "Marangoni and Gravity Driven Convection in a Liquid Layer Overlying a Porous Layer: Lateral and Bottom Heating Conditions", *Energy Sources, vol. 27, pp. 151-171*, 2005.

[2] D. A. Nield, A. Bejan, Convection in Porous Media, Springer-Verlag: New York, 1992.

[3] D. A. Nield, "Onset of convection in a Fluid Layer Overlying a Layer of porous Medium", *J. Fluid Mech. 81* (1977) 513-522.

[4] R. V. Birikh, "Thermocapillary Convection in a Horizontal Layer of Liquid, *J. of Applied Mechanics and Technical Physics", Vol. No. 3, pp. 69-72*, 1966.

[5] D. Villers and J. K. Platten, "Coupled buoyancy and Marangoni convection in acetone: experiments and comparison with numerical simulations", *J. Fluid Mech. vol. 234, pp. 487-510*, 1992.

[6] J. R. A. Pearson, "On convection cells induced by surface tension", 1958.

[7] R. Kozak, M.Z. Saghir, and A. Viviani, "Marangoni convection in a liquid layer overlying a porous layer with evaporation at the free surface", *Acta Astronautica, vol. 55, pp. 189-197*, 2004.

[8] H. B. Hadid and B. Roux, "Thermocapillary convection in long horizontal layers of low-Prandtl-number melts subject to a horizontal temperature gradient", *J. Fluid Mech. vol. 221, pp. 77-103,* 1990.

[9] D. Schawabe, A. Cramer, J. Scheneider, S. Benz and J. Metzger, "Experiments on the multi-roll-structure of thermocapillary flow in side-heated thin liquid layers", *Adv. Space Res. vol. 24, no. 10, pp. 1367-1373,* 1999.

[10] D. Schwabe, "The Benard-Marangoni-instability in small circular containers under microgravity: experimental results", *Adv. Space Res. vol. 24, no. 10, pp. 1347-1356,* 1999.

[11] N. F. M. Mokhtar, N. M. Arifin, R. Nazar, F. Ismail, and M. Suleiman, "Marangoni Convection in a Fluid Saturated Porous Layer with a Prescribed Heat Flux at its Lower Boundary".

[12] A. Bahloul, R. Delahaya, P. Vasseur, and L. Robillard, "Effect of Surface Tension on Convection in a Binary Fluid Layer Under Zero Gravity Environment", *International Journal of Heat and Mass Transfer, vol. 46, pp. 1759-1771*, 2003.

[13] A. Delache, M. N. Ouarzazi, "Weakly nonlinear interaction of mixed convection patterns in porous media heated from below", *International Journal of Thermal Sciences, vol. 47, pp. 709-722,* 2008.

[14] P. Kandaswamy, M. Eswaramurthi, "Density Maximum Effect on Buoyancy-Driven Convection of Water in a Porous Cavity with Variable Side Wall Temperature", *International Journal of Heat and Mass Transfer, vol. 51, pp. 1955-1961*, 2008.

[15] S. J. Kim and C. Y. Choi, "Convective heat transfer in porous and overlying fluid layers heated from below", *Int. J. Heat Mass Transfer, vol. 39, no. 2, pp. 319-329,* 1996.

[16] F. Chen and C.F Chen, "Experimental investigation of convective stability in a superposed fluid and porous layer when heated from below", *J. Fluid Mech. vol. 207, pp. 311-321,* 1989.

[17] T. Deasaive, G. Lebon and M. Hennenberg, "Coupled capillary and gravity-driven instability in a liquid film overlying a porous layer", *Phy. Rev. E, vol. 64,* 2001.

[18] I. S. Shivakumara, S.P. Suma, K. B. Chavaraddi, "Onset of surface-tension-driven convection in superposed layers of fluid and saturated porous medium", *Arch. Mech., vol. 58, 2, pp. 71-92,* Warszawa 2006.

[19] M. K. Smith, and S. H. Davis, "Instabilities of dynamic thermocapillary liquid layers. Part 1. Convective instabilities", *J. of Fluid Mech, vol. 132, pp. 119-144*, 1983.

[20] K. Hooman, and H. Gurgenci, "Effects of Temperature-Dependent Viscosity on Benard Convection in a Porous Medium Using a Non-Darcy Model", *Int. J. of Heat and Mass Transfer, vol. 51, pp. 1139-1149,* 2008.

[21] A. Silberstein, C. Langlais, and E. Arquis, "Natural Convection in Light Fibrous Insulating Materials with Permeable Interfaces: Onset Criteria and Its Effect on the Thermal Performances of the Product", *Journal of Thermal Insulation, vol. 14, pp. 22-42,* July, 1990.

[22] M. Z. Saghir, M. Hennenberg, and M. R. Islam, "Double Diffusive and Marangoni Convection in a Multi-Cavity System", *Int. J. of Heat Mass Transfer, vol. 41, no. 14, pp. 2157-2174,* 1998.

[23] J. Tanny and B. Yakubov, "Experimental study of a double-diffusive two-layer system in a laterally heated enclosure", *Int. J. of heat and mass transfer, vol. 42, pp. 3619-3629,* 1999.

[24] C. G. Jiang, M. Z. Saghir, M. Kawaji, and K. Ghorayeb, "Two-dimensional numerical simulation of thermo-gravitational convection in a vertical porous column filled with a binary fluid mixture", *Int. J. of thermal Science, vol. 43, pp. 1057-1065,* 2004.

[25] A. Bergeon, D. Henry, H. Benhadid, and L. S. Tuckerman, "Marangoni convection in binary mixtures with Soret effect", *J. Fluid Mech. vol. 375, pp. 143-177,* 1998.

[26] A. Mansour, A. Amahmid, and M. Hasnaoui, "Soret effect of thermosolutal convection developed in a horizontal shallow porous layer salted from below and subject to cross fluxes of heat", *Int. J. of Heat and Fluid Flow, vol. 29, pp. 306-314,* 2008.

[27] C. G. Jiang, T. J. Jaber, H. Bataller, and M. Z. Saghir, "Simulation of Ludwig-Soret effect of a water-ethanol mixture in a cavity filled with aluminum oxide powder under high pressure", *Int. J. of thermal Science, vol. 47, pp. 126-135,* 2008.

[28] L. B. Benano-Melly, J.-P. Caltagirone, B. Faissat, F. Montel and P. Costeseque, "Modeling Soret coefficient measurement experiments in porous media considering thermal and solutal convection", *International Journal of Heat and Mass Transfer, vol. 44, pp. 1285-1297,* 2001.

[29] J. K. Platten, "The Soret effect: A review of recent experimental results", *J. of Applied Mechanics, vol. 73, pp. 5-15,* 2006.

[30] D. v. Alexandrov, and D. L. Aseev, "Directional solidification with a two-phase zone: thermodiffusion and temperature-dependent diffusivity", *Computational Materials Science, vol. 37, pp. 1-6,* 2006.

[31] M. Er-Raki, M. Hasnaoui, A. Amahmid, and M. E. Ganaoui, "Specific behavior of thermosolutal convection induced in a vertical porous medium in the case of a separation coefficient identical to the ratio of buoyancy forces", *C. R. Mechanique, vol. 336, pp. 304-312,* 2008.

[32] L. Ming-chun, T. Yan-wen, "Soret and Dufour effects in strongly endothermic chemical reaction system of porous media", *Trans nonferrous Mot. Soc. vol. 16, pp. 1200-1204*, 2006.

[33] FIDAP USER MANUAL, Volume 8.7.0, 1999.

[34] F. M. White, Viscous Fluid Flow 2nd Edition, McGraw-Hill Series in Mechanical Engineering, 1991.

[35] F. M. White, Fluid Mechanics 6th Edition, McGraw-Hill Higher Education, New York, 2006.

[36] J. J. Jasper, "The Surface Tension of Pure Liquid Compounds", *Journal of Physical and Chemical Reference Data, vol. 1, No. 4, pp. 841-1010,* 1972.

[37] V. Shevtsova, D. Melnikov, J. C. Legros, Y. Yan, M. Z. Saghir, T. Lyubimova, G. Sedelnicov, B. Roux, "Influence of vibrations on thermodiffusion in binary mixture: A benchmark of numerical solutions", *Physics of Fluids, vol. 19, 017111*, 2007.